ARTICLE IN PRESS

Journal of Geodynamics xxx (xxxx) xxx–xxx

Contents lists available at ScienceDirect

Journal of Geodynamics

journal homepage: www.elsevier.com/locate/jog

A simple toy model for coupled retreat and detachment of subducting slabs

David Bercovici*, Elvira Mulyukova, Maureen D. Long

Department of Geology & Geophysics, Yale University, New Haven, CT, USA

ARTICLE INFO

Keywords:
Plate tectonics
Trench retreat
Slab detachment
Damage mechanics

ABSTRACT

Subducting slabs are the primary drivers of plate tectonics and mantle circulation, but can also undergo various instabilities that cause dramatic adjustments in tectonic evolution and motion. Slab rollback or trench retreat is possibly a dominant form of time dependence in the plate-mantle system, causing plates to shrink and the mantle to undergo complex flow patterns. Likewise, slab detachment can induce abrupt adjustments in both plate motions and vertical displacement of continents. The arrival or accumulation of continental crust over a subduction zone induces high stresses on the plate and slab that can trigger either rollback or detachment or both. However, these processes necessarily interact because of how stress is relieved and plate motions altered. Here we present a simple boundary-layer like model of coupled trench retreat and slab detachment, induced by continent accumulation, and with slab necking augmented by grain-damage self-weakening (to allow for abrupt necking). With this model we find that, with continental accumulation, initial rollback is at first modest. However, as the stress from continental accumulation peaks, it triggers abrupt slab detachment. The subsequent slab loss causes the plate to lose its primary motive force and to thus undergo a more dramatic and rapid rollback event. After the larger rollback episode, the contracted continental mass re-expands partially. Plausible grain-damage parameters and 40 km thick crust cause abrupt detachment and major rollback to occur after a few hundred million years, which means the plates remain stable for that long, in agreement with the typical age for most large plates. While the complexity of some field areas with a well documented history of detachment and rollback, such as the Mediterranean, taxes the sophistication of our toy model, other simpler geological examples, such as on the western North American plate, show that episodes of rollback can follow detachment.

1. Introduction

Mantle convection on Earth is most clearly expressed by subducting slabs, where tectonic plates or lithosphere becomes sufficiently cold and heavy to sink into the hot underlying mantle, thereby cooling it off (e.g., Schubert et al., 2001; Bercovici et al., 2015b; Wada and King, 2015). Subduction is, moreover, accepted as the main driving force for horizontal plate motion (Forsyth and Uyeda, 1975; Schubert, 1980; Vigny et al., 1991), as well as vertical tectonic adjustment (Gurnis, 1990, 1993). Subduction zones are also subject to various instabilities, most notably trench retreat by slab foundering or roll-back, and slab detachment by tearing or necking. Both phenomena have dramatic consequences on horizontal and vertical tectonics.

Slab rollback can strongly affect mantle flow patterns, as determined by seismic anistropy, back-arc volcanism, and the shape of subduction zones (Lallemand et al., 2008; Clark et al., 2008; Long and Silver, 2009; Stegman et al., 2010; Long et al., 2012; Crameri and Tackley, 2014). One of the most basic causes for rollback is excess negative buoyancy (i.e., weight) of the surface plate (Stegman et al., 2010), although other conditions exist (see Stegman et al., 2006, 2010; Schellart et al., 2007, 2008; Clark et al., 2008), and the evolution of trench retreat is a function of, for example, plate strength, trench strike length, and resistive mantle flow (Kincaid and Griffiths, 2003; Funiciello et al., 2006; Piromallo et al., 2006; Stegman et al., 2010; Gerya and Meilick, 2011). The negative buoyancy of the plate can be increased by any effect that slows the plate down, which causes it to cool and grow heavy enough to become convectively unstable before it reaches its trench. Plates can slow down if, for example, their driving slab impinges on a viscosity increase in the lower mantle (e.g., Billen and Hirth, 2007; Billen, 2008), although this effect can also be offset if the slab piles up or thickens on entry into the lower mantle by viscous inflation (e.g., Gurnis and Hager, 1988) or by folding (Ribe, 2003; Ribe et al., 2007; Lee and King, 2011). An endothermic phase transition at the 660 km boundary can impede slab penetration into the lower mantle as well (e.g., see Schubert et al., 1975; Tackley et al., 1993; Bercovici et al., 1993). The arrival or accumulation of continental crust at a subduction zone can also congest it, and cause the plate velocity to decrease and trigger rollback (e.g., Moresi et al., 2014; Bercovici and

* Corresponding author.
E-mail addresses: david.bercovici@yale.edu (D. Bercovici), elvira.mulyukova@yale.edu (E. Mulyukova), maureen.long@yale.edu (M.D. Long).

https://doi.org/10.1016/j.jog.2018.03.002
Received 23 August 2017; Received in revised form 4 March 2018; Accepted 9 March 2018
0264-3707/

Please cite this article as: Bercovici, D., Journal of Geodynamics (2018), https://doi.org/10.1016/j.jog.2018.03.002

Long, 2014).

Subducting slabs can also undergo necking and detachment from their trailing plate (see Schmalholz, 2011; Duretz et al., 2012 Duretz et al., 2012). Slab detachment is possibly evident in subduction seismicity gaps and tomographically inferred pinching of slab structures (Wortel and Spakman, 2000; Rogers et al., 2002). Detachment has also been invoked to cause abrupt changes in plate motion, as well as fast uplift (e.g., see Duretz et al., 2012; Bercovici et al., 2015a, and references therein). Slab detachment is generally observed to be rapid, on the order of a few million years; however, numerical models using basic olivine creep rheologies typically find that cold, strong slabs detach in tens of millions of years (Schott and Schmeling, 1998; van Hunen and Allen, 2011), unless additional effects are incorporated. Such effects include, for example, softening by viscous heating (Gerya et al., 2004), multiple lithologies with independent rheological laws, including Peierls creep for very high stress-low temperature conditions (Duretz et al., 2011, 2012), or implicit weak zones (Burkett and Billen, 2010). In the same vein, Bercovici et al. (2015a) showed that slabs could abruptly detach in a few million years with a grain-damage mechanism (Bercovici and Ricard, 2012) that greatly accelerates necking in the slab.

Despite much progress in modeling slab rollback and slab detachment, each process is often treated as if it occurs independently. In particular, the subduction of thickened crust can trigger both rollback and detachment, but it is not always clear which of the two processes would dominate or occur first and to what extent they influence each other. Models that have included post-collisional delamination of the lithosphere from continental crust with subsequent roll-back and slab detachment find that the timing of these processes depends strongly on the various ways in which the lithosphere and crust are mechanically coupled (Ueda et al., 2012; Magni et al., 2013).

Here, we develop and explore a simple boundary-layer-like toy model to illustrate the coupling and relative timing of slab rollback and necking after the arrival or accumulation of thickened crust over a subduction zone. Since the dominant retarding force on plate motion is assumed to come from drag and congestion by continental crust at the surface, the model does not account for all the possible causes of rollback (e.g., from slabs stalling in the transition zone) or detachment (e.g., pinning of slabs at the termini of their arc). For instances in which continental accumulation is the root cause for these phenomena, our model suggests that rollback and necking occur sequentially in three phases: at first there is a modest rollback caused by the initial drag of the accumulating continent, and then when continental drag or congestion peaks, abrupt detachment occurs, after which the loss of a motive slab force causes the plate velocity to drop and the plate to founder and rollback. The conditions for these events, as well as their timing and characteristics, can be easily interrogated given the simplicity of the model.

2. Theory

Our model couples several components involving surface motion of an evolving plate that is itself pulled by a slab that can undergo necking and detachment (Fig. 1). Continental crustal thickness and breadth also evolve according to the accumulation of crust over a subduction zone. Buoyant crust congests the subductive downwelling by adding resistance to both plate motion and slab descent, and this then triggers rollback and necking. Lastly, the necking of the slab is facilitated and accelerated by grain-damage, wherein grain reduction driven by deformation and damage causes weakening through grain-size sensitive rheology (Bercovici and Ricard, 2012; Bercovici et al., 2015a).

2.1. Plate length and trench position

In our simple model (as also in Bercovici and Long, 2014), subduction occurs where the top thermal boundary layer, i.e., the

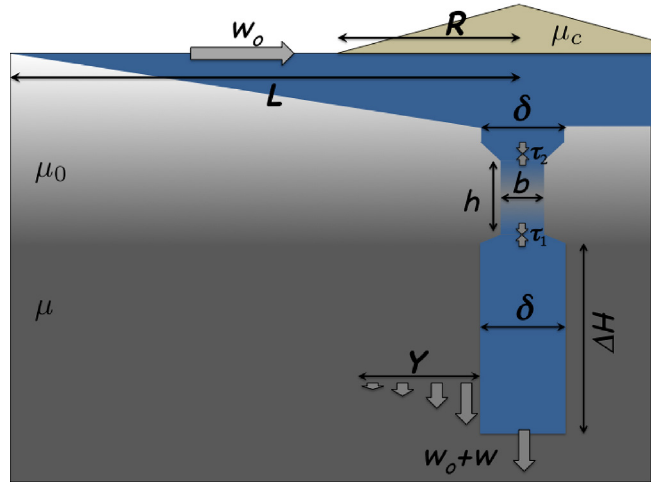

Fig. 1. Schematic cartoon of the model geometry and some of its key parameters and variables. See text and Table 1 for definitions of various quantities.

lithosphere, goes convectively unstable, which is parametrically equivalent to the condition for when the slab is heavy enough to sink against viscous resistance. Thus, the thickness of the subducting slab δ is determined when the local Rayleigh number for the boundary layer equals the critical Rayleigh number for the onset of convection (Howard, 1966; Solomatov, 1995):

$$\frac{2\Delta\rho g\delta^3}{\mu_0\kappa} = \mathrm{R}_c \tag{1}$$

where g is gravity, $\Delta\rho = \frac{1}{2}\rho\alpha_v\Delta T$ is the average lithosphere and slab density anomaly in which ρ is mantle density, α_v thermal expansivity, ΔT the lithospheric temperature drop, μ_0 the upper-mantle viscosity (which first resists the instability), κ thermal diffusivity, and $\mathrm{R}_c \approx 660$ is the critical Rayleigh number for a free-slip surface (Chandrasekhar, 1961). In this case, δ is a system constant (and using typical mantle properties from Table 1, $\delta \approx 80$ km, which is well within observed ranges). However, since (1) is a parametric condition for the plate's gravitational instability it is only approximate; i.e., the value of R_c might differ from the classical value of 660, but probably not by orders of magnitude, since the critical Rayleigh number for most convective systems is typically $O(10^3)$.

Given a plate and slab velocity w_0, the length of the plate to the subduction zone would, in a steady-state, arise from the relation for the thermal boundary layer thickness $\delta = 2\sqrt{\kappa L_0/w_0}$ (Turcotte and Oxburgh, 1967) or that

$$L_0 = \frac{\delta^2}{4\kappa}w_0 \tag{2}$$

(which, again using mantle properties from Table 1 and a typical plate velocity $w_0 \approx 5$ cm/yr, yields $L_0 \approx 2000$–3000 km; this is also well within the observed ranges for plate length). If the plate velocity w_0 slowed down because of a change in the force balance on it (see Section 2.3), the plate length would shorten, but not necessarily immediately since it would take some time for the plate to cool and thicken (although an instantaneous response was assumed by Bercovici and Long, 2014). Nevertheless, we assume that even as it shortens, the edge that subducts (i.e., the edge that is negatively buoyant enough to sink) still has thickness close to δ.

To consider how the plate length L adjusts to a change to a new plate velocity w_0, we consider a segment of the upper mantle of depth d that includes the lithosphere and the entire plate of length L from ridge to trench; thus the segment is bounded by the domain $0 < x < L$ and $-d < z < 0$ (Fig. 2). At any given x the thickness of the lithosphere is $\bar{\delta}(x) \le \delta$, and at that x, the temperature is given by

Table 1
Dimensional material and model properties.

Quantity	Symbol	Value
Density, mantle	ρ	$3300\,\mathrm{kg/m^3}$
Density, continent	ρ_c	$2700\,\mathrm{kg/m^3}$
Gravitational acceleration	g	$10\,\mathrm{m/s^2}$
Thermal expansivity	α_v	$3\times10^{-5}\,\mathrm{K^{-1}}$
Lithosphere temperature drop	ΔT	$1400\,\mathrm{K}$
Thermal diffusivity	κ	$10^{-6}\,\mathrm{m^2/s}$
Viscosity, upper mantle	μ_0	$10^{21}\,\mathrm{Pa\,s}$
Viscosity, mean mantle	μ	$30\mu_0$
Viscosity, continent	μ_c	$5\times10^{19}\,\mathrm{Pa\,s}$
Viscosity, trench	μ_T	$\mu/10$
Mantle depth	D	$3000\,\mathrm{km}$
Continent thickness	h_c	$40\,\mathrm{km}$
Continent 2-D volume	V	$\mathrm{h}_c D/3$
Initial slab width	δ	$80\,\mathrm{km}$
Initial slab length	H_0	$1500\,\mathrm{km}$
Mantle velocity decay length	Y	H_0
Initial slab neck length	$h_0=\alpha\delta$	$\alpha=2$
Disloc. creep compliance	A	$3.6\times10^{-42}\,\mathrm{s^{-1}\,Pa^{-n}}$
Disloc. creep stress exponent	n	3
Diff. creep compliance	B	$2.3\times10^{-35}\,\mathrm{s^{-1}\,Pa^{-1}\,m^{m}}$
Diff. creep grainsize exponent	m	3
Grain/interface coarsening rate	G	$3.4\times10^{-38}\,\mathrm{m^{q}\,s^{-1}}$
Grain/interface coarsening exponent	q	4
Interface surface tension	$\mathfrak{s}$	$1\,\mathrm{Pa\,m}$
Damage partitioning fraction	f	10^{-3}
Phase mixture coefficient	η	0.72

Olivine creep laws from Hirth and Kohlstedt (2003), using $n=3$ instead of $n=3.5$. Grain/interface-coarsening law from Bercovici et al. (2015a) after Bercovici and Ricard (2012, 2013), with an activation energy of $E_g=300\,\mathrm{kJ/mol}$. Damage fraction law from Rozel et al. (2011) but using a lower value of $\mathrm{f}_0=2\times10^{-3}$ at $T=1000\,\mathrm{K}$ as suggested by Mulyukova and Bercovici (2017). All these laws are evaluated at $T=1100\,\mathrm{K}$ and pressure $P=5\,\mathrm{GPa}$.

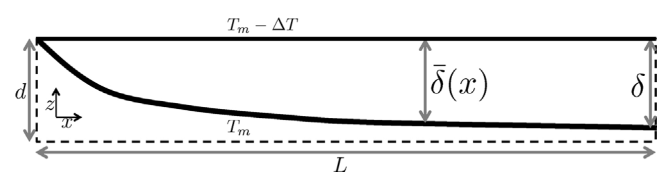

Fig. 2. Sketch for the model of plate length evolution. See Section 2.1 for further description.

$$T(x,z)=\begin{cases}T_m-\Delta T(1+z/\bar{\delta}(x)) & \text{for } -\bar{\delta}\le z\le 0\\ T_m & \text{for } z\le-\bar{\delta}\end{cases} \tag{3}$$

The plate moves at velocity w_0 and we assume the mantle beneath it (to depth d) moves at a similar velocity. The energy balance on the entire segment is given by

$$\frac{\partial}{\partial t}\int_0^L\int_{-d}^0 T\,\mathrm{d}x\,\mathrm{d}z=-\int_{-d}^0 Tw_0\,\mathrm{d}z\Big|_{x=0}^{L}+\int_0^L\kappa\frac{\partial T}{\partial z}\mathrm{d}x\Big|_{z=0} \tag{4}$$

where conductive heat flow to the base of the plate is zero since the underlying mantle is isothermal. We further assume that to leading order $\bar{\delta}(x)\approx 2\sqrt{\kappa x/w_0}$, which means that the plate thickness is close to that for an equilibrium thermal boundary layer. Carrying through the integrals and assuming that only L is a function of time, (4) leads first to

$$\left(T_m d-\frac{\Delta T}{2}\delta\right)\dot{L}=\frac{\Delta T}{2}w_0\delta-2\frac{\kappa\Delta T}{\delta}L \tag{5}$$

where we assume in the final evaluation of terms that $2\sqrt{\kappa L/w_0}\approx\delta$, which implies that L is not too far from the equilibrium length L_0. The segment depth d is arbitrary and there is no need for it be deeper than δ, thus we can assume $d=\delta$. Moreover, we can assume the surface temperature $T_m-\Delta T=0$. Thus (5), with (2), leads to

$$\dot{L}=w_0-\frac{4\kappa}{\delta^2}L=\frac{4\kappa}{\delta^2}(L_0-L) \tag{6}$$

Note that this simple linear relation is only accurate to first order and assumes the changes in velocity are not so rapid that the plate length deviates very far from its equilibrium length L_0. However, like all linearized disequilibrium equations, the relation captures the essential physics in that the plate length tends to converge toward its equilibrium state. Of course, trench migration and subduction age on Earth are certainly more complex than (6) implies. Subduction zone ages have, for example, a wide distribution, including zero ages (see Becker et al., 2009), although even this enigmatic observation is not inconsistent with thermal convection and boundary-layer heat loss in the mantle (Labrosse and Jaupart, 2007; Coltice et al., 2012). But in total, our simple model displays the basic process whereby if the plate slows down, it then cools, and subsequently shortens as the slab rolls back.

2.2. Continental accumulation and resistance

We next consider the accumulation of a finite 2-D volume of buoyant unsubductable continental "fluid" of thickness h, density ρ_c and viscosity μ_c, under the action of plate motion sweeping it toward a subduction zone. This process was developed previously by Bercovici and Long (2014), but we follow a somewhat different direction than that study and thus summarize the essential physics here.

The evolution of the continental mass can be captured by a simple model for a viscous 2-D gravity current of thickness h with a free-slip surface and a no-slip base moving at a horizontal velocity of the underlying plate $v(x)$ (where $v(x)=w_0$ away from the trench, but goes to 0 at the trench position $x=L$) is

$$\frac{\partial \mathrm{h}}{\partial t}+v\frac{\partial \mathrm{h}}{\partial x}=\frac{\rho' g}{3\mu_c}\frac{\partial}{\partial x}\left(\mathrm{h}^3\frac{\partial \mathrm{h}}{\partial x}\right)-\mathrm{h}\frac{\partial v}{\partial x} \tag{7}$$

(Huppert, 1982) where $\rho'=(\rho-\rho_c)\rho_c/\rho$ is the isostatically reduced crustal density (Didden and Maxworthy, 1982). The continental gravity current is assumed to have an approximately self-similar shape peaking at the convergence zone at $x=L$ and is given by $\mathrm{h}(x,t)=\mathrm{H}(t)f(\zeta)$, where $\zeta=(x-L)/R$ (i.e., to the left of the slab $\zeta<0$), H is the characteristic height, f is a dimensionless shape function, and R is the half-length of the current's base (Fig. 1). The current's volume is conserved, thus the half-volume (per unit length into the plane) $V=\mathrm{H}(t)R(t)\int_{-1}^0 f(\zeta)\mathrm{d}\zeta$ is a constant; we can define $\int_{-1}^0 f\mathrm{d}\zeta=1$ such that $\mathrm{H}(t)=V/R(t)$. As shown later, the fluid mass spends most of "model time" near its steady state, and we thus assume its shape $f(\zeta)$ is close to that of the steady critical wedge in which the advection term on the left balances the gravity collapse (i.e. nonlinear diffusion) term on the right of (7). Satisfying the volume integral constraint on f, we find $f(\zeta)\approx\frac{4}{3}(1+\zeta)^{1/3}$ for $\zeta<0$. Substituting $\mathrm{h}=\frac{V}{R}f(\zeta)$ into (7), evaluating it near the edge of the gravity current ($\zeta\approx-1$) where we assume $dv/dx\approx0$ (i.e., that the current's edge is sufficiently far from the convergence zone) and $v\approx w_0$, we obtain the rate of change of width of the continental mass

$$\dot{R}=\frac{c\rho' g V^3}{\mu_c}\frac{1}{R^4}-w_0 \tag{8}$$

where $c=2^6/3^5\approx0.26$. (We note that this is a different condition than assumed in Bercovici and Long (2014), wherein (7) was evaluated at $\zeta=0$, which causes overly rapid continent convergence.) This equation simply says that the current's edge migrates in toward the subduction zone initially at the plate speed, until the current piles up enough that its upper layers flow back against the direction of plate motion, eventually approaching a critical wedge shape.

2.2.1. Continental drag and viscosity

The stress of the continental gravity current acting against the top of the plate is $\tau_c=-\rho' g\mathrm{h}\frac{\partial h}{\partial x}$ and the force (per unit length into the plane) acting against the plate is

$$F_c = \int_{L-R}^{L} \tau_c \,\mathrm{d}x = -\frac{8\rho' g V^2}{9R^2} \tag{9}$$

The treatment of the continent as a viscous gravity current is of course a significant simplification that is meant to capture the net gravitational collapse of the continental mass by crustal flow, failure, and erosion (e.g., Rey et al., 2001). Moreover, the rheology of crustal material is far more complicated than that of a viscous fluid (Meissner, 1986; Kirby and Kronenberg, 1987; Kohlstedt et al., 1995Meissner, 1986; Kirby and Kronenberg, 1987; Kohlstedt et al., 1995 Kohlstedt et al., 1995). Thus the effective continental viscosity μ_c is a parameterization of multiple effects, and it is instructive to estimate its value from first order observations of continent size.

Given a steady-state half-width R_0, the half-volume of continental mass is $V = h_c R_0$, where h_c is the average thickness of continental crust. The steady state solution to (8) thus suggests the continent viscosity would be

$$\mu_c = \frac{c\rho' g V^3}{R_0^4 w_0} = \frac{c\rho' g h_c^3}{R_0 w_0} \tag{10}$$

Assuming a convection cell has width equivalent to the mantle depth D, then a steady-state Earth-like continent would cover approximately 1/3 of this width such that $R_0 \approx D/3$ (i.e., in principle a full continent of width $2R_0$ sits between two convection cells of total width $2D$ and covers 1/3 of this width). Using Earth-like values for various mantle and material properties (Table 1), and a typical plate velocity of $w_0 \approx 5$cm/yr, we find $\mu_c \approx 5 \times 10^{19}$Pa s, which is a plausible enough number for effective viscosity of continental crust (e.g., see Clift et al., 2002; Vergnolle et al., 2003).

2.3. Force balance on the plate

The horizontally moving tectonic plate (Fig. 1) experiences several motive and retarding forces. The subducting slab pulls on the plate, but in our model this is due to stress transmitted to the plate from the necking portion of ths slab, with a force (per length into the plane) of $\tau_2 b$, where τ_2 is the normal stress at the top of the neck and b is the width of the neck (Fig. 1). This stress transmission does not necessarily require the slab to be strong, since even a weak but tabular heavy sinker extending to the subduction zone will transmit stress to the surface by fluid tractions and a surface low pressure zone (e.g., see Tao and O'Connell, 1993). (There are other caveats associated with our stress-transmission assumption, which are discussed later in Section 2.6.1, since they also affect other components of the model.) The classical so-called ridge push force, which is actually due to gravitational sliding from the ridge is well approximated by $\rho\alpha_v \Delta T \kappa L/w_0 \approx \Delta\rho g\delta^2/2$ (Turcotte and Schubert, 2014). The force of viscous resistance to plate motion likely has two components. First, the force of drag along the base of the plate from shear stresses in the asthenosphere is approximately $\mu_a w_0 L/d_a$ (where μ_a and d_a are the viscosity and effective depth of the asthenosphere). Second, the force of resistance to bending the plate through the subduction zone (e.g., see Conrad and Hager, 2001; Buffett, 2006; Buffett and Rowley, 2006; Buffett and Becker, 2012) is approximately $2\mu_T w_0$ (where μ_T is the effective trench viscosity), which is the normal stress associated with the plate velocity going from w_0 to 0 over approximately a width δ, multiplied by the area of the surface on which it acts (per length into the page) δ. However, the asthenospheric drag is likely negligible relative to other forces because μ_a is much less than the mantle viscosity μ through which the slab descends, and the geometric factor L/d_a is unlikely to be large enough to compensate for this (e.g., see Richards et al., 2001). The resistance to bending is not likely to be negligible, however, as the plate is already weak enough to subduct, we assume this resistance is not overwhelming or dominant. In total, and including the continental drag force (9), the total force balance on the plate is simply

$$\tau_2 b + \Delta\rho g\delta^2/2 - 2\mu_T w_0 - \frac{8\rho' g V^2}{9R^2} = 0 \tag{11}$$

2.4. Mechanical work balance on the detaching slab

On the other end of the necking portion of the slab (which we'll deal with shortly) is the detaching portion of the slab itself. The original length of the slab before necking occurs is H_0 and the initial length of the necking portion is h_0; assuming the detaching portion does not deform appreciably after necking ensues, it has a fixed length $\Delta H = H_0 - h_0$ (Fig. 1). Assuming that the detached slab remains undeformed is equivalent to assuming that it never impinges on the core-mantle boundary (CMB) within the time of the calculation; if the model treated impingement on the CMB, then the detached slab would shorten and slow down as it falls, and thus likely reduce the rate of necking.

The detaching slab descends vertically at a velocity $w_0 + w$, where w is the excess velocity due to stretching of the necking region. The slab also potentially experiences lateral motion as the trench retreats (or advances as the case may be) at a rate $\dot{L}$, which is thought to induce mantle motion and drag; in the case where 3-D motion is allowed, toroidal motion around the slab possibly occurs (see Long and Becker, 2010). Rather than account for all modes of force balances, we consider (as in Bercovici and Long, 2014) the balance of mechanical work on the detaching slab, i.e., the rate of release of its gravitational potential energy balanced by the rates of viscous work done by the mantle on either side of the slab, and the work of the necking region pulling up on the detaching slab. The total energy balance is

$$\begin{aligned}\Delta\rho g\Delta H\delta\ (w_0 + w - \dot{L}) = \tau_1 b(w_0 + w) + 2\mu(w_0 + w)^2\Delta H/Y \\ + 4\gamma\mu\dot{L}^2\Delta H/Y\end{aligned} \tag{12}$$

where the various terms warrant some explanation. The gravitational energy release on the left side of (12) has a contribution from the gravitational work at the normal descent rate $w_0 + w$; however, if the trench recedes at a rate of $-\dot{L}$, then the slab swings down and drops a distance $|dL|$ in time dt, thereby releasing additional gravitational energy (see also Bercovici and Long, 2014). The work from the necking portion (first term on the right side of (12)) is due to the stress at the base of the neck τ_1 pulling up across a width b (see Fig. 1) against the slab's vertical descent. The viscous drag against vertical descent (second term on the right of (12)) is due to shear stress in the mantle acting on both vertical faces of the slab, where μ is the mantle viscosity (typically the lower mantle viscosity), and the induced velocity in the mantle is assumed to decay away over a length Y (again, see Fig. 1). Finally, the viscous "paddle" drag from the slab pulled in the wake of slab rollback and trench retreat (last term on the right of (12)) is due to horizontal normal viscous stresses in the mantle acting on both vertical faces of the slab (the induced mantle flow is assumed to also decay over a length Y). The fraction γ accounts for how much of the mantle is involved with resistance to rollback; e.g., if portions of the slab are anchored in the transition zone or lower mantle then they participate less in rollback, in which case γ is small.

2.5. Force balance, rheology and damage in the slab neck

The necking portion of the slab undergoes stretching, and in the process, weakening by simple grain damage, which was shown by Bercovici et al. (2015a) to allow for the rapid detachment often associated with abrupt changes in plate motion and vertical uplift. The necking portion initially starts out with a length h_0 and width δ and as it stretches the evolving length $h(t)$ increases and the width $b(t)$ decreases. However, once necking starts we assume it is rapid enough that the neck remains near the top of the slab, and also that mass and thus volume of the necked region are approximately conserved, hence $h(t)b$

$(t) = h_0\delta$; i.e., in the interval of time of the necking instability, the subduction of the trailing plate does not significantly add mass to the necking region or push it to greater depth. Our assumption that the neck is connected to the surface plate at all times leads to a few limitations and caveats, as discussed further in Section 2.6.1

The initial length of the necking region h_0 is given by a necking instability such that $h_0 = \alpha\delta$ (see Bercovici et al., 2015a), in which case $hb = \alpha\delta^2$. Values of α are greater than 1 and can reach up to about 5 (see Bercovici et al., 2015a) depending on the initial rheology of the slab and surrounding mantle; here we assume an intermediate value of $\alpha = 2$ and a slab of initially moderate extent into the lower mantle e.g., $H_0 = 1500$ km, which give plausible initial tectonic velocities, and are consistent with our assumptions about drag on the sides of the neck (see below). A choice of large α and larger H_0 yield similar results.

The evolution of the width of the necking portion is given by conservation of its volume $hb = \alpha\delta^2$ and that $\dot{h} = w$, which immediately leads to

$$\dot{b} = -\frac{b^2}{\alpha\delta^2}w \tag{13}$$

The forces on the necking portion include its relative weight pulling down, and the action of stresses at its top τ_2 and bottom τ_1 pulling up and down, respectively. The force balance on the neck is therefore

$$-\Delta\rho g\alpha\delta^2 + (\tau_2 - \tau_1)b = 0 \tag{14}$$

where we have replaced the volume (per length along the trench) of the necking portion hb with $\alpha\delta^2$. We have neglected the drag on the vertical sides of the necking portion of the slab for simplicity and with two means of justification. First, during the initial stages of necking, that portion of the slab is likely to be surrounded by low viscosity asthenosphere, which provides little drag (or, similarly, non-Newtonian mantle rheology causes the rapidly deforming corner-flow regions on either side of the slab to have low viscosity; see, e.g., Billen and Hirth, 2007; Billen, 2008; Jadamec and Billen, 2010, 2012). Second, once necking ensues, that slab portion can pass into the lower, more viscous part of the mantle, but by then grain-size reduction by damage occurs, and the viscosity of the necking portion itself drops, again leading to little drag on the sides. The complexity of adding this term is thus unwarranted (unless α is large enough to extend the initial necking region into the lower mantle).

The deformation and rheology of the necking portion itself is given by a composite rheology and constitutive law, as in Bercovici et al. (2015a) (see also Billen and Hirth, 2007; Billen, 2008):

$$\dot{e} = \frac{w}{h} = \frac{\mathrm{wb}}{\alpha\delta^2} = A\bar{\tau}^n + B\frac{\bar{\tau}}{r^m} \tag{15}$$

where $\dot{e}$ is the normal vertical strain-rate, $\bar{\tau} = \frac{1}{2}(\tau_1 + \tau_2)$ is the mean stress in the neck, A and B are the dislocation and diffusion creep compliances, respectively, n is the dislocation creep exponent, which we assume is $n = 3$, r is the effective grain-size for a polymineralic mixture whose grain-size evolution is dominated by Zener pinning (see below), and m is the grain-size exponent that we assume is also typically $m = 3$ for Coble diffusion creep.

The grain-size evolution in the neck is given by the simplified version of the full two-phase grain-damage theory of Bercovici and Ricard (2012) as used in Bercovici et al. (2015a):

$$\dot{r} = \frac{\eta G}{\mathrm{q}r^{q-1}} - \frac{\mathrm{f}r^2}{\mathfrak{s}\eta}\left(A\bar{\tau}^{n+1} + B\frac{\bar{\tau}^2}{r^m}\right) \tag{16}$$

where G is the effective grain coarsening rate, q is an effective grain-growth exponent, which for this two-phase system is typically $q = 4$; η depends on the phase fraction of the polymineralic mixture but is typically of order $\eta = 0.72$ for a 40–60 mixture of olivine and pyroxene for a lithospheric (upper-mantle) peridotite; f is the fraction of deformational work going toward creating surface energy on the interface between the phases, and $\mathfrak{s}$ is the surface tension on this same interface.

The evolution equation (16) is actually for the coarsening of the interface between mineral phases, where strictly speaking r is the radius of curvature of the interface. Here we assume that, because of Zener pinning, the grains in either mineral phase become slave to the evolution of the interface, whose curvature dictates the efficacy of pinning (Bercovici and Ricard, 2012), and thus only the interface evolution need be tracked. For this same reason, the grain-size is kept proportional to r and, for a mantle peridotite mixture, it is typically of order $\pi r/2$ (see Bercovici and Ricard, 2012, 2016; Bercovici et al., 2015a). The damage partitioning fraction f can also include a parameterization for an inter-phase mixing transition at small grain-sizes, which leads to a hysteresis or threshold effect in the equilibrium grains-size with increasing stress (Bercovici and Ricard, 2016; Bercovici and Skemer, 2017; Mulyukova and Bercovici, 2017); however for the sake of simplicity and focus, we neglect that effect in this study.

2.6. Dimensionless governing equations

There are eight dimensional governing equations. These include four instantaneous response equations for the force and/or work balance on the plate, slab and neck, and the neck rheology, (11), (12), (14), (15), respectively. These are coupled to four evolution equations for the plate length, continent width, neck width and neck grainsize (6), (8), (13) and (16), respectively.

Given the number of coupled governing equations and parameters, it is useful to nondimensionalize the system of equations by their intrinsic length, time and stress scales. We first nondimensionalize macroscopic quantities of length such that $(L, R, b) = \delta(\mathrm{u}, \mathrm{R}, \mathrm{b})$, time by $\delta^2/(4\kappa)$, and thus velocity according to $(w_0, w) = (4\kappa/\delta)(\mathrm{w}_0, \mathrm{w})$. We also nondimensionalize stress to match the initial (dislocation creep) strain-rate scale to the inverse time scale, such that $\tau = \check{\tau}\tau'$, where

$$\check{\tau} = \left(\frac{4\kappa}{\delta^2 A}\right)^{1/n} \tag{17}$$

in which, for example, given characteristic material properties (Table 1), $\check{\tau} = 560$ MPa. The grain-size is nondimensionalized according to $r = \check{r}\mathrm{r}$, where $\check{r} = B/(A\check{\tau}^{n-1})$ is the grain-size at the field boundary between diffusion and dislocation creep for the given stress scale $\check{\tau}$; given the characteristic $\check{\tau}$, the grain-size scale is $\check{r} = 270$ μm. Using these definitions, the eight dimensionless governing equations become (dropping the primes on τ)

plate force balance: $$\tau_2\mathrm{b} + \frac{1}{2}\mathscr{B} - \eta_{\mathrm{T}}\mathrm{w}_0 - \frac{\mathscr{C}}{\mathrm{R}^2} = 0 \tag{18a}$$

slab work balance: $$\mathscr{B}\Delta\mathscr{H}(\mathrm{w}_0 + \mathrm{w} - \dot{\mathrm{u}}) - \tau_1\mathrm{b}(\mathrm{w}_0 + \mathrm{w}) - \eta_{\mathrm{M}}(\mathrm{w}_0 + \mathrm{w})^2 - 2\gamma\eta_{\mathrm{M}}\dot{\mathrm{u}}^2 = 0 \tag{18b}$$

neck force balance: $$(\tau_2 - \tau_1)\mathrm{b} - \mathscr{B}\alpha = 0 \tag{18c}$$

neck rheology: $$\mathrm{wb} = \alpha\left(\bar{\tau}^n + \frac{\bar{\tau}}{\mathrm{r}^m}\right) \tag{18d}$$

trench migration: $$\dot{\mathrm{u}} = \mathrm{w}_0 - \mathrm{u} \tag{18e}$$

continent width evolution: $$\dot{\mathrm{R}} = \frac{\mathscr{K}^4}{\mathrm{R}^4} - \mathrm{w}_0 \tag{18f}$$

neck width evolution: $$\dot{\mathrm{b}} = -\mathrm{b}^2\mathrm{w}/\alpha \tag{18g}$$

neck grainsize evolution: $$\dot{\mathrm{r}} = \frac{\mathscr{G}}{q\mathrm{r}^{q-1}} - \mathscr{D}\mathrm{r}^2\left(\bar{\tau}^{n+1} + \frac{\bar{\tau}^2}{\mathrm{r}^m}\right) \tag{18h}$$

(see Table 2 for a summary of dependent variables) where

$$\mathscr{B} = \frac{\Delta\rho g\delta}{\check{\tau}}\quad,\quad \mathscr{C} = \frac{8\rho' g V^2}{9\check{\tau}\delta^3} \tag{19a}$$

$$\eta_{\mathrm{T}} = \frac{8\mu_{\mathrm{T}}\kappa}{\check{\tau}\delta^2}\quad,\quad \eta_{\mathrm{M}} = \frac{8\mu\kappa}{\check{\tau}\delta^2}\frac{\Delta H}{Y} \tag{19b}$$

Table 2
Dependent model variables.

Quantity	Dimensional symbol	Dimensionless symbol
Plate length	L	u
Continent breadth	R	R
Slab neck width	b	b
Neck effective grain-size	r	r
Plate velocity	w_0	w_0
Detaching slab relative velocity	w	w
Stress, top of neck	τ_2	τ_2
Stress, bottom of neck	τ_1	τ_1
Mean neck stress	$\bar{\tau} = \frac{1}{2}(\tau_1 + \tau_2)$	$\bar{\tau}$

Table 3
Dimensionless model parameters as defined in (19), using material properties from Table 1, and dimensional scales defined in Section 2.6.

Quantity	Symbol	Characteristic value
Slab and plate negative buoyancy	$\mathscr{B}$	0.09
Detached slab length	$\Delta\mathscr{H}$	17
Initial slab neck length	α	2
Mantle resistance	η_M	0.06
Trench resistance	η_T	0.007
Retreating slab paddle factor	γ	0.2
Continent drag	$\mathscr{C}$	24
Continent collapse rate	$\mathscr{K}$	30
Grain/interface coarsening	$\mathscr{G}$	7×10^{-9}
Grain/interface damage	$\mathscr{D}$	200
Disloc. creep stress exponent	n	3
Diff. creep grainsize exponent	m	3
Grain/interface coarsening exponent	q	4

$$\Delta\mathscr{H} = \Delta H/\delta \quad , \quad \mathscr{K}^4 = \frac{c\rho' g V^3}{4\kappa\mu_c\delta^3} \tag{19c}$$

$$\mathscr{G} = \frac{\mathfrak{y} G\delta^2}{4\kappa\breve{r}^q} \quad , \quad \mathscr{D} = \frac{\mathfrak{f}\breve{r}\breve{\tau}}{\mathfrak{s}\mathfrak{y}} \tag{19d}$$

(see Table 3). The general solution strategy is to solve the instantaneous response equations (18a)–(18d) in order to write w_0, w, τ_1 and τ_2 (and hence $\bar{\tau}$) as functions of u, R, b and r; these functions are then used in (18e)–(18h), with given initial conditions, to evolve the widths of the plate, continent and neck (u, R, and b) and the grain-size (*r*).

2.6.1. Limitations and caveats of model assumptions

As the model is described, e.g., in final dimensionless form in (18), the slab neck is always assumed to be the topmost portion of the slab, and directly coupled to the surface plate through the stress τ_2. The model does not account for any new, un-necked slab that sinks into the mantle after necking begins, by either normal subduction and/or slab roll-back. This effect would lead to new slab material that either trails the necking portion of the slab, or flows into the neck as it stretches and sinks. While this is not an unfeasible model feature, it leads to an excessively complex description of the dynamics and rheological response of the slab neck that belies the purpose of this simple toy model. Thus we opt to limit the model to conditions whereby the slab neck is of constant volume, and remains near the top of the slab and connected to the subduction hinge. Therefore, strictly speaking, the model only applies for a short period of time after necking ensues, which is most applicable for rapid necking, as occurs when there is grain-damage and self-weakening (as already demonstrated by Bercovici et al., 2015a, and also shown in the results below). Once the detached slab is effectively lost by necking, the new nearly slabless plate slows down abruptly (as shown below in Sections 3.2 and 3.3), now driven only by ridge push, before subducting further, or undergoing trench retreat. The equilibrium plate length associated with this slower speed (e.g., $\mathrm{u} = \mathrm{w}_0$ in (18e)) indicates the minimum length to which the plate could shrink. This minimum length could be reached if, for example, new slab subducting after the initial necking event continues to break off (e.g., because of its excess negative buoyancy) thus keeping the plate effectively slabless. However, one might equally expect any newly subducting slab to augment the plate's speed, and so the plate would not necessarily retreat to this minimum length, but would instead retreat a lesser amount. Given this limitation of the model, one of our primary foci is on the retreat velocity $\dot{\mathrm{u}}$ (or dimensionally $\dot{L}$) soon after necking occurs, as a diagnostic of how necking influences roll-back. Even so, we will display the absolute plate length u (or L) for the cases in which retreat follows necking, but with the understanding that the final steady state is a lower bound on the length of the retreating plate.

The model also does not include an explicit thick, strong and buoyant continental lithosphere that mirrors the continental mass. The effect of continental resistance and congestion is entirely contained in the treatment of the continental gravity current. Thus, if continental congestion causes the plate to slow down in our model, the trench retreats continuously beneath the accumulated continent. In reality, continental lithosphere would be unsubductable and trench retreat from the continental congestion would more likely be discontinuous and jump to the margin with oceanic lithosphere via the initiation of a new subduction zone.

Finally, we note that "trench retreat" is assumed equivalent to slab roll-back and refers to the absolute motion of the subduction zone itself (relative to the ridge; see Fig. 2); it is not associated with the movement of the ocean-continent margin, which can migrate if the continental mass contracts or spreads.

3. Analysis and results

Although our model is effectively a toy model, there are still a sufficient number of equations and parameters to make it complicated enough (see Table 3). Rather than attempt to explore a ten-dimensional parameter space (8 from (19) along with γ and α, which is slightly better than the dimensional system which has 4 extra dimensions of parameter space), we opt to fix the reasonably well-constrained dimensionless parameters given available data, and then explore the effects of some of the lesser-constrained ones. Moreover, we also tune or select some parameters, like trench resistance η_T, to give plausible results, such as plate velocity w_0. These choices will become evident as we explore some simple end-member cases.

3.1. Simple case 1: rollback only

For the system with only trench retreat, we prescribe that the necking velocity $\mathrm{w} = 0$ while the neck width remains fixed at $\mathrm{b} = 1$. In this case only (18a)–(18c), (18e) and (18f) are necessary to describe the system.

3.1.1. Steady-state solutions

The steady state to this system represents continuous subduction without roll-back and exists when $\dot{\mathrm{u}} = \dot{\mathrm{R}} = 0$, and thus $\mathrm{u} = \mathrm{w}_0$ from (18e); the combination of (18a)–(18c) with (18f) leads to

$$(\eta_M + \eta_T)\mathrm{u} + \frac{\mathscr{C}}{\mathscr{K}^2}\mathrm{u}^{1/2} - \mathscr{B}\left(\Delta\mathscr{H} + \alpha + \frac{1}{2}\right) = 0 \tag{20}$$

A simple but instructive limit to this system is one for an initial quasi-steady state in which $\mathrm{R} \rightarrow \infty$ (the continent is spread thinly and nearly uniformly) leading to negligible continental resistance on the plate, which is effectively equivalent to setting $\mathscr{C} \approx 0$ in (20); this yields

$$\mathrm{u} = \mathrm{w}_0 = \frac{\mathscr{B}\left(\Delta\mathscr{H} + \alpha + \frac{1}{2}\right)}{\eta_M + \eta_T} \tag{21}$$

with which we can glean some constraints on the effective dimensionless trench viscosity η_T. In particular, most of the other parameters in (21) are well constrained (Table 3) and we find that unless η_T is significantly less than η_M the initial plate velocity is unrealistically slow, of order 1 cm/yr or less (when redimensionalized by $4\kappa/\delta$), which is slow for a plate connected to a slab. For $\eta_T \approx 0.1\eta_M$ the plate velocity is typically of order 5 cm/yr. Although we do not show it here, values of $\eta_T \geq \eta_M$ induce excessive stresses in the plate and slab and trigger necking almost immediately, while $\eta_T \to 0$ precludes necking from occurring in a geologically (let alone astronomically) reasonable time frame. Overall choosing $\eta_T \approx 0.1\eta_M$, permits physically plausible results and suggests that the trench has to be effectively about as weak as the upper mantle (whose strength is represented by the dimensionless number $\eta_M \mu_0/\mu = \eta_M/30$; see also Foley et al., 2012; Mulyukova and Bercovici, 2018). This weakening could have been due to subduction initiation with weakening effects such as grain-damage rheology (e.g., see Mulyukova and Bercovici, 2018) or some other form of failure associated with slab seismicity (Bevis, 1986, 1988); either way, we assume here that subduction is past initiation and that the weakening which allowed subduction is already well developed.

It is also worth pointing out that the other steady solution in the limit $t \to \infty$ and thus $\dot{\mathsf{R}} = 0$, for $\mathscr{C} \neq 0$, in (20) is the root to a quadratic polynomial for the variable $\mathsf{x} = \mathsf{u}^{1/2}$. However it suffices to note that since the term proportional to $\mathscr{C}$ in (20) is positive it necessarily yields solutions for u and w_0 less than those for (21), depending on $\mathscr{C}/\mathscr{K}^2$. These solutions can be seen in the full analysis of the evolution equation.

3.1.2. Evolution

The evolution equations for rollback can be determined by combining (18a)–(18c) to get a quadratic polynomial for w_0

$$\tilde{a}\mathsf{w}_0^2 - \tilde{b}\mathsf{w}_0 - \tilde{c} = 0 \text{ where} \tag{22a}$$

$$\tilde{a} = \eta_M(1 + 2\gamma) + \eta_T \tag{22b}$$

$$\tilde{b} = \mathscr{B}\left(\alpha + \frac{1}{2}\right) - \mathscr{C}/\mathsf{R}^2 + 4\gamma\eta_M \tag{22c}$$

$$\tilde{c} = \mathsf{u}(\mathscr{B}\Delta\mathscr{H} - 2\gamma\eta_M\mathsf{u}) \tag{22d}$$

The positive root to (22) gives the function $\mathsf{w}_0(\mathsf{u}, \mathsf{R})$, with which we can integrate (18e) and (18f) to get the evolution of u and R in time (Fig. 3, which is shown in dimensional quantities for ease of reference). The solutions to (22) also provide some constraints on γ to guarantee that the roots are always real, i.e., that the solution's radicand $\tilde{b}^2 + 4\tilde{a}\tilde{c} > 0$. However, to avoid gratuitous and tiresome math, suffice it to say that only a large γ can cause complex roots, and thus we infer it is significantly less than 1; in the end provided $\gamma \sim O(0.1)$ the solutions are well behaved and real; we generally set $\gamma = 0.2$, although this has little net effect other than modest adjustment of the initial rollback step (Fig. 3).

The results of the rollback-only model show that contraction of the continent, and associated build-up of continental drag on the plate, triggers modest trench retreat to a slightly smaller and slower steady-state plate. As the continent contracts the mean stress $\bar{\tau}$ on the neck of the slab is given by 2·(18a)–(18c), leading to

$$\bar{\tau}\mathsf{b} = \eta_T\mathsf{w}_0 + \mathscr{C}/\mathsf{R}^2 - \frac{1}{2}\mathscr{B}(\alpha + 1) \tag{23}$$

where we have left the factor of b (despite the fact that, for this case, it is not necking and thus b = 1) on the left side for future reference, since this way (23) applies generally to all cases. Eq. (23) displays the contributions to stress from viscous resistance at the trench and continental drag, with some offset by ridge push and weight of the slab neck (both inside the term proportional to $\mathscr{B}$). Overall, the stress on the neck is positive and only increases because of continent contraction, since all other terms in (23) are constant or shrinking. In particular, for the simple case considered (Fig. 3), the continent contracts from about 2000 km to 1000 km in roughly 50 Myrs, during which time the mean stress increases from about 40 MPa to 90 MPa. The increase in stress triggers modest trench retreat, which reaches a peak rollback speed of only 1.2 mm/yr, but the rollback is completed well after the continent has contracted. In particular, for our simple case, rollback causes the plate length to go from about 2120 km to 1960 km (for a net shortening a bit less than 200 km, i.e., about 10%) and slows from 4.2 cm/yr to 3.9 cm/yr. The rollback is complete in about 300 Myrs, which is similar to that for a typical Wilson cycle over which, as suggested by Bercovici and Long (2014), accumulation of a continent might naturally trigger dispersal by rollback; although with this simplest possible case the rollback is small. However, as we will show below (Section 3.3), when rollback and slab necking are coupled the rollback is potentially far more dramatic. Finally we note that in light of the model limitations described in Section 2.6.1, the plate-driving force of the foundering portion of the slab, which results from rollback, is excluded from the model; however, as rollback is modest at best, this is unlikely to have significant effect.

3.2. Simple case 2: necking only

For the case in which the slab undergoes necking but does not roll back, we simply assume the plate length u remains fixed and thus $\dot{\mathsf{u}} = 0$. In this case, we employ all the governing equations (18) except for (18e) for the roll-back rate. The constant plate length u is given by the starting steady-state length (21).

3.2.1. A brief note on the solution approach

Given the number of equations it is worth briefly summarizing the basic solution approach. First, taking the sum of (18a) and (18b) (with a factor of $(\mathsf{w}_0 + \mathsf{w})$ removed since $\dot{\mathsf{u}} = 0$), and eliminating $\tau_2 - \tau_1$ with (18c) leads to an equation for the plate velocity

$$\mathsf{w}_0 = \frac{\mathscr{B}\left(\Delta\mathscr{H} + \alpha + \frac{1}{2}\right) - \mathscr{C}/\mathsf{R}^2 - \eta_M\mathsf{w}}{\eta_M + \eta_T} \tag{24}$$

(Note in the limit of $\mathsf{R} \to \infty$ and $\mathsf{w} = 0$, the above equation is the same as that for the initial steady state plate (21).) This relation shows that while the plate's motion is driven in total by slab pull and ridge push (the term proportional to $\mathscr{B}$), it is being resisted by continental drag, and is losing motive force as the slab detaches at a relative velocity w. (However, as discussed in Section 2.6.1, this relation mostly applies during and immediately after abrupt necking, since it does not account for the effect of newly subducted slab following the necking event.) The expression for $\bar{\tau}$ is identical to that in (23). The relations for $\bar{\tau}$ and w_0 can be used together in the neck rheology relation (18d) to yield a polynomial equation for w, which can be solved to give the functions w (R, b, r) and thus implicitly w_0(R, b, r) and $\bar{\tau}$(R, b, r). These three functions are then used in (18f)–(18h) to evolve R, b and r.

3.2.2. Evolution

The steady state solutions to this system do no strictly exist since there is no steady state limit to the necking rate relation (18g). The time dependent solutions to (18) are determined numerically with stiff ordinary differential equation solvers (e.g., in Matlab) and yield a remarkably different evolution than in the case with only roll-back (Fig. 4, shown with dimensional variables). As with the roll-back case, the continent contracts and induces a climb in stress on the slab and plate within about 50 Myrs, which causes the plate to start slowing down at the same time (shown by a reduction in w_0). The climb in stress also begins to drive initial grain-size reduction in the slab neck, and this grain-size reaches the diffusion creep regime in about 200 Myrs. Up to that point the slab remains un-necked and the relative necking velocity w is negligible. But once the grain-size hits the field boundary between diffusion and dislocation creep (see Fig. 4), at about 200 Myrs, necking begins to ensue abruptly, accelerating grain-size reduction further into diffusion creep and thus causing rapid weakening of the neck. The

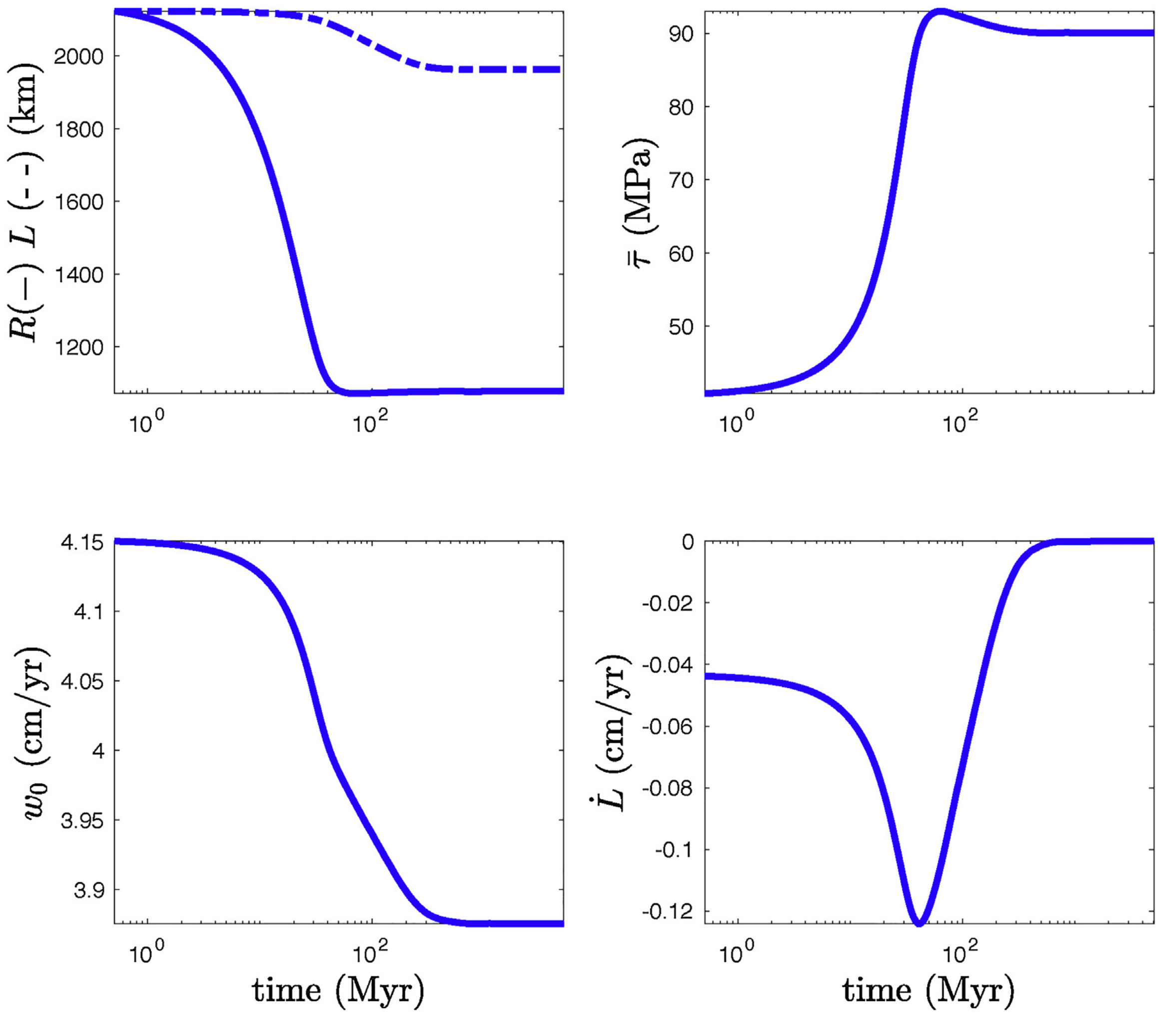

Fig. 3. Rollback only case shows (top left) plate length L (dashed curve) and continent breadth R (solid curve); (top right) mean stress on the slab $\bar{\tau}$; (bottom left) plate velocity w_0; and (bottom right) roll-back rate $\dot{L}$, versus time. The case shown is for continental mean thickness $h_c = 40$ km and viscosity $\mu_c = 5\times10^{19}$ Pa s. All quantities shown are dimensional, wherein the dimensionless variables u, R, τ, w_0, and $\dot{u}$ are redimensionalized by $\delta = 80$ km for length, $\check{\tau} = 560$ MPa for stress, $4\kappa/\delta = 1.6$ mm/yr for velocity, and $\delta^2/(4\kappa) = 51$ Myrs for time. The initial conditions on the dimensionless plate length u and continent width R are both given by (21).

relative necking velocity w jumps abruptly, while the plate velocity w_0 drops equally abruptly; the total velocity of the detaching slab is $w_0 + w$, which basically goes toward the Stokes settling velocity for the detached slab. After the stress initially increases in the slab and plate, it drops precipitously once the slab detaches and its weight is supported by background mantle drag.

The initial small spike in w, before it settles to a stable value, occurs because of the precipitous plunge in grain-size r once it crosses the field-boundary from dislocation to diffusion creep. At this point the viscosity is grain-size dependent and decreases rapidly while the stress in the neck is still large, causing rapid necking and a peak in w. However, the subsequent drop in stress as the slab detaches causes the necking rate and w to decrease slightly and stabilize.

Finally, while the continent initially contracts under the initial plate motion, and that contraction triggers the events to follow, the drop in plate velocity causes the continent to expand again to a new steady state size, suggestive of continent dispersal. However, we have not accounted for new slab to be subducted after necking, at the new slower plate velocity w_0, and so the results apply up to times immediately after the slab is detached.

3.3. Coupled necking and rollback

The coupling of slab rollback and necking is described by the full set of governing equations (18) for which we evolve all variables including plate length u, continent breadth R, slab neck width b and effective grain-size r.

3.3.1. Another brief note on the solution approach

The full system of equations is significantly more complex and nonlinear than the two previous limiting cases of either isolated roll-back or necking. In general, we used (18a)–(18d) to obtain w, w_0 and $\bar{\tau}$ as functions of b, R and r, which can then be used to integrate the evolution equations (18e)–(18h). Specifically, taking the sum of $(w_0 + w)\cdot$(18a) and (18b), and eliminating $\tau_2 - \tau_1$ with (18c) and $\dot{u}$ with (18e) leads to the polynomial

$$\breve{a}(w_0 + w)^2 - \breve{b}(w_0 + w) - \breve{c} = 0 \text{ where} \quad (25a)$$

$$\breve{a} = \eta_M(1 + 2\gamma) + \eta_T \quad (25b)$$

$$\breve{b} = \mathscr{B}\left(\alpha + \frac{1}{2}\right) - \mathscr{C}/R^2 + 4\gamma\eta_M(w + u) + \eta_T w \quad (25c)$$

$$\breve{c} = (u + w)(\mathscr{B}\Delta\mathscr{H} - 2\gamma\eta_M(u + w)) \quad (25d)$$

the solution of which gives w_0 as a function of w, along with the evolving variables u and R. The mean stress $\bar{\tau}$ is found in exactly the same manner as described in Section 3.2.1, and gives $\bar{\tau}$ as a function of w_0 (along with evolving variables b and R). The function $\bar{\tau}(w_0(w))$ is

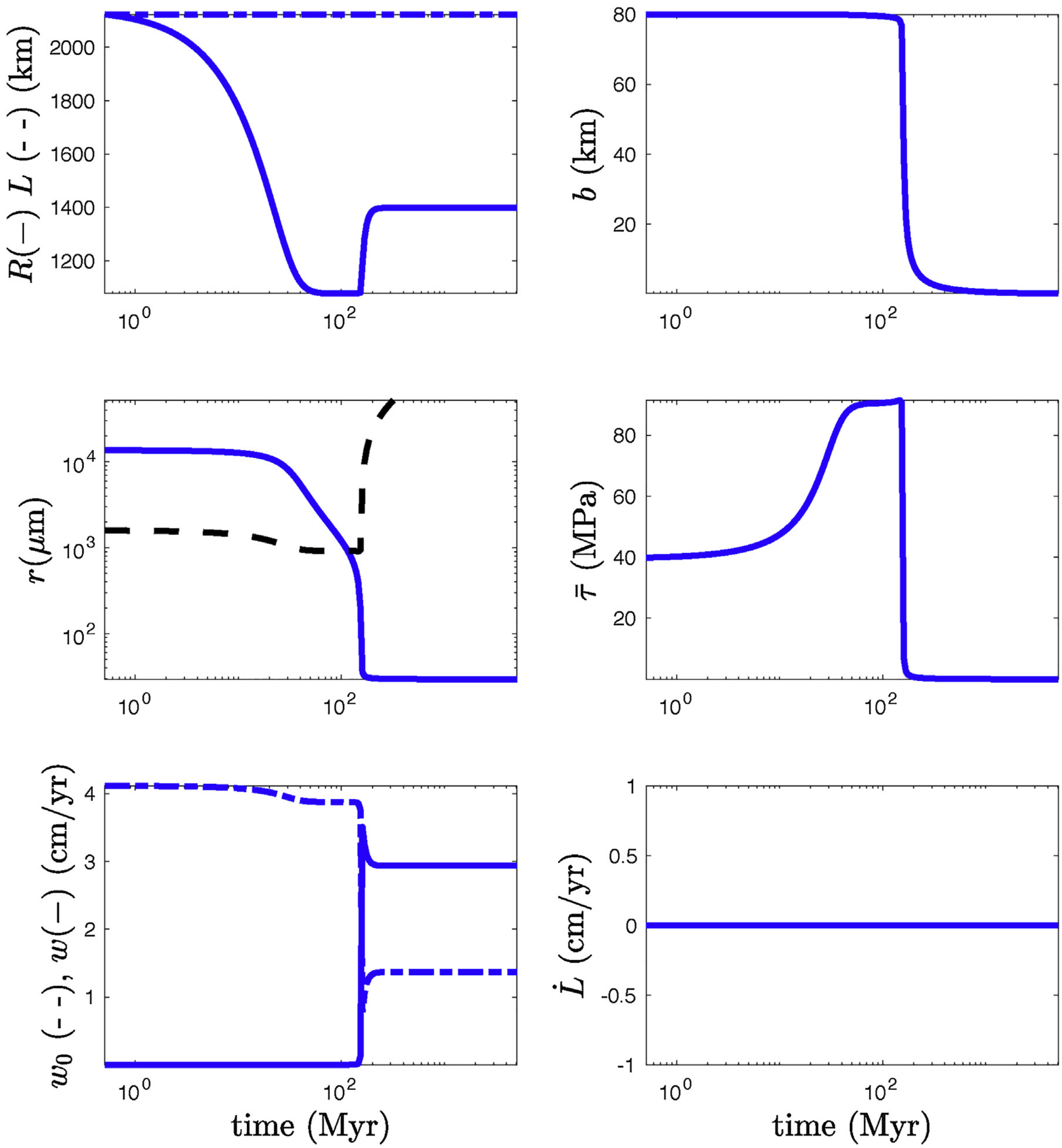

Fig. 4. Slab necking only case shows dimensional (top left) plate length L (dashed) and continent breadth R (solid); (top right) neck width b; (mid left) effective grain-size in the neck r; (mid right) mean stress in the neck $\bar{\tau}$; (bottom left) plate velocity w_0 (dashed) and relative detaching slab velocity w (solid) where the full slab velocity is $w_0 + w$; and (bottom right) trench retreat rate $\dot{L}$. The plot of r versus t also shows the field-boundary $r_f = (B/A)\bar{\tau}^{(1-n)/m}$ (black dashed curve), which delineates the transition from dislocation creep ($r > r_f$) to diffusion creep ($r < r_f$). Information about redimensionalization is the same as in Fig. 3, with the additional information that b is dimensionalized by δ, and the grain-size by $\check{r}$ = 273 μm. Dimensionless numbers for the calculation are shown in Table 3. Initial conditions on the dimensionless system are the same as in Fig. 3, in addition to b = 1 and r = 50. (For interpretation of the references to color in this figure legend, the reader is referred to the web version of the article.)

then used in (18d) to yield a polynomial equation for w, which can be solved to give the functions w(u, R, b, r) and thus implicitly w_0(u, R, b, r) and $\bar{\tau}$(u, R, b, r), which are then used in (18f)–(18h) to evolve u, R, b and r.

3.3.2. Evolution

As with the case for isolated necking (Section 3.2) there is no true steady state solution b to (18g). The time dependent solutions to (18) are determined as with the necking-only case. Indeed, the evolution of the coupled system differs modestly from the necking-only scenario, with a few notable differences (Fig. 5, which is displayed in dimensional quantities). As expected, the breadth of the continent R (or dimensionally R) contracts and induces a climb in stress on the slab and plate within about 50 Myrs (for the primary set of model parameters in Table 3; see Fig. 5 blue curves), which causes the plate velocity w_0 (dimensionally w_0) to decrease, and hence an initial modest trench retreat reflected in the reduction of plate length u (dimensionally L) as in the roll-back-only model (Section 3.1). As in the necking-only model, the climb in stress eventually triggers abrupt necking in about 200 Myrs (Fig. 5 blue curves). Moreover, as a result of necking, the plate velocity w_0 (or w_0) drops rapidly, which then triggers a relatively rapid episode of trench retreat at a speed $\dot{u}$ (or $\dot{L}$) that is comparable to tectonic speeds, at greater than 3 cm/yr, which is much larger than in the case without necking. However, as noted in Section 2.6.1, the final length u or L to which the plate recedes is a lower bound, since we have not accounted for the effect of newly subducted slab following necking,

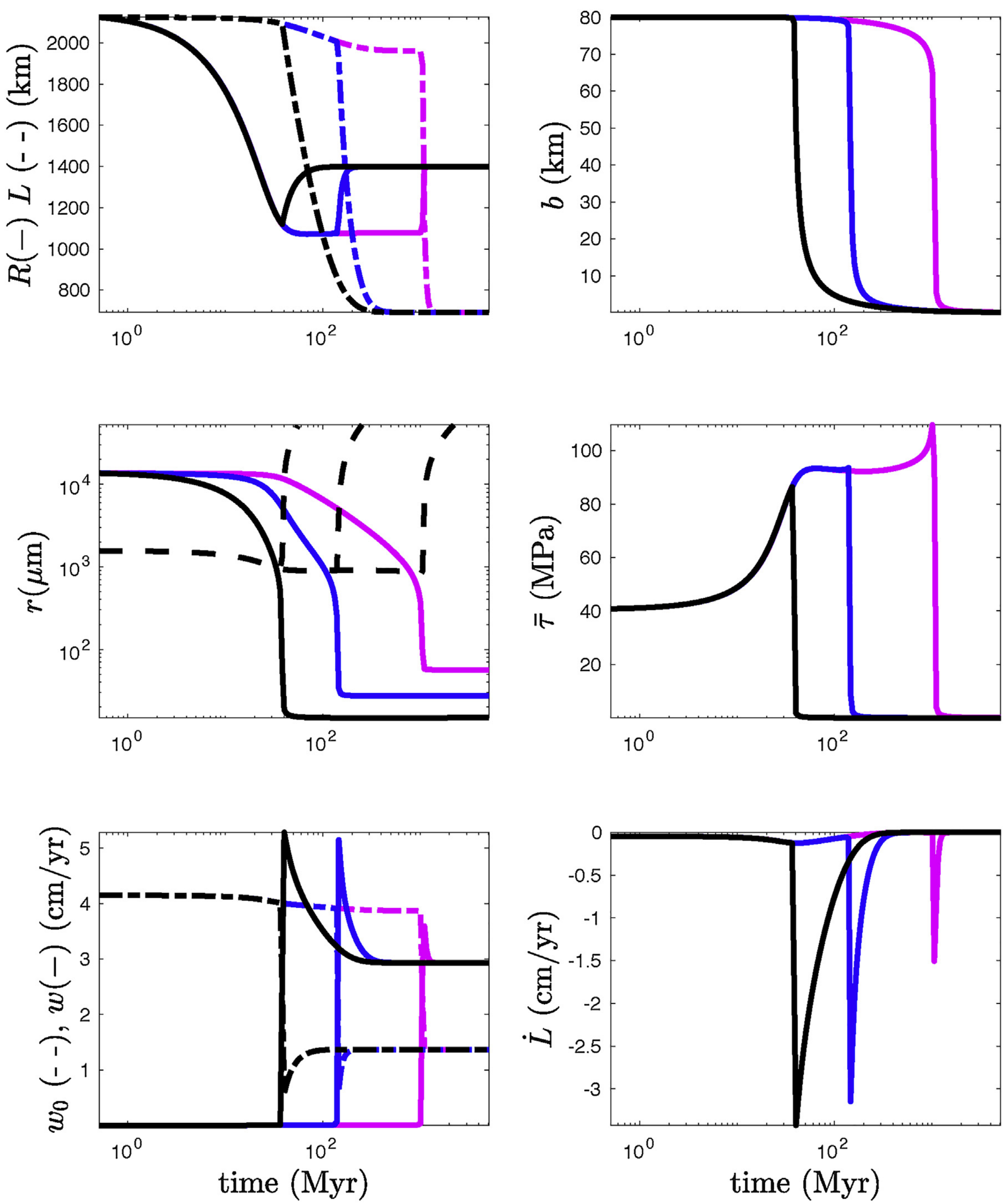

Fig. 5. Coupled slab necking and roll-back case shows the evolution of the same quantities described in Fig. 4. Colored curves show different damage numbers, specifically, $\mathscr{D} = 20$ (magenta), 200 (blue) and 2000 (black). Information about redimensionalization and initial conditions are the same as in Fig. 4. (For interpretation of the references to color in this figure legend, the reader is referred to the web version of the article.)

which would augment the speed of the plate after it lost its original slab. As in the necking-only case, the continent initially contracts and then re-expands partially after the slab necks.

One of the most notable differences between the fully coupled case and the necking-only case is the dramatic effect that necking has on trench retreat. The abrupt reduction in the slab pull force after necking occurs causes the plate velocity to drop by nearly a factor of 3, and thus the plate undergoes a relatively rapid episode of retreat, causing the plate length to reduce also by a factor of 3, from about 2000 km to about 700 km (but without accounting for newly subducted slab, which would partially mitigate the extent of retreat and plate shortening). Moreover, the initial jump in relative necking velocity w is more dramatic for the fully coupled case before it settles down to its stable value; this jump is inferred to be due to the initial rollback motion, which causes the slab to release gravitational potential energy more rapidly, which briefly contributes to the descent rate of the entire slab.

3.3.3. Effect of grain-damage

Although there are various controlling parameters (Table 3), most of them are reasonably well constrained. However, the grain-evolution parameters $\mathscr{G}$ and $\mathscr{D}$ are least constrained since they actually pertain to the coarsening rate G and damage partitioning fraction f on the interface between phases, for which there is only indirect experimental information. The interface coarsening rate has been inferred from laboratory experiments on synthetic peridotites (Hiraga et al., 2010; Bercovici and Ricard, 2012) and is generally much slower than grain-growth in a pure phase like olivine (Karato, 1989; Evans et al., 2001), hence the very small dimensionless value of $\mathscr{G}$. If $\mathscr{G}$ is made much larger, then the evolution in r would show a growth and recovery in effective grain-size that would be basically the steady state solution to (18h) (since grain-growth would be fast enough to keep pace with the dropping stress). However, this would require about a 6 or 7 orders of magnitude increase in $\mathscr{G}$ to effect this change, which is implausible. Thus we leave the exploration of $\mathscr{G}$ alone and note that it causes r to appear to flatten in time after stress has dropped because it is, in fact, recovering, albeit very slowly.

The grain damage $\mathscr{D}$ is less constrained because empirical measurements for the damage partitioning fraction f are indirect at best. The damage partitioning fraction for pure olivine can be inferred from paleopiezometer measurements, provided that other experimental data for creep rheology and grain growth are available (Rozel et al., 2011; Mulyukova and Bercovici, 2017). This olivine partitioning fraction is an important baseline and shows that typical f values are very small (10^{-4}–10^{-3}) at temperatures around 1000 K (Mulyukova and Bercovici, 2017). However, the damage process for these partitioning fractions is only for generation of dislocations and subgrain formation during dynamic recrystallization (Karato et al., 1980; Austin and Evans, 2007; Rozel et al., 2011), and may have little to do with damage to the interface between phases in the polymineralic mixture, which does not undergo dynamic recrystallization but is more likely due to distortion and tearing of the interface and inter-phase grain mixing (Linckens et al., 2014; Cross and Skemer, 2017; Bercovici and Skemer, 2017). Thus, there is some flexibility in our estimates of f. For the primary set of model parameters (Tables 1 and 3) we choose $f = 10^{-3}$ at temperature $T = 1100$K, and thus the dimensional damage number $\mathscr{D} = 200$. To explore some range in the damage partitioning we also consider f and $\mathscr{D}$ an order of magnitude on either side of these primary values (which are consistent with those inferred by Bercovici and Ricard, 2016, in comparison to field data), i.e., $\mathscr{D} = 20$ and 2000 (Fig. 5 magenta and black curves). The effect of lowering or raising $\mathscr{D}$ by an order of magnitude is essentially to make necking, and the resulting behavior, happen later or earlier, respectively. For $\mathscr{D} = 2000$ necking occurs in about 50 Myrs, before the continent is even done contracting. For $\mathscr{D} = 20$ necking does not occur until about 1 Gyr. In contrast, the primary value of $\mathscr{D} = 200$ leads to necking in about 200 Myrs. Since tectonic plates typically remain stable for a few 100 Myrs, and that few major plates are as young as a few 10 s of Myrs, while none are of order 1 Gyr old, then the intermediate and primary value of $\mathscr{D}$ seems most plausible.

3.3.4. Effect of crustal thickness

In our model, the contraction of the continent causes the accumulation of stress by continental drag against the plate, that eventually triggers first slow roll-back, and then abrupt necking followed by more dramatic trench retreat, and concomitant deceleration of the plate and re-spreading of the continent. However, the stress induced is necessarily related to the mass or volume V of the continent that piles up over the subduction zone and eventually pushes back as it acts to collapse against the motion of the plate (see Section 2.2.1). The primary set of parameters for this study employ a mean continent thickness (when it covers 1/3 of the surface) of $h_c = 40$ km (see Table 1). In these cases, and with plausible enough choices of other parameters, the stress from continent contraction builds up to about 90 MPa and triggers necking and dramatic roll-back by about 200 Myrs. However, if the crustal thickness is much thinner, e.g., at the end member typical of oceanic crust of $h_c < 10$ km, then the stress accumulation is about half as much as for 40 km thick crust, and necking and rollback are not triggered until about 1 Gyr and with much slower peak trench retreat speeds $\dot{L}$ (Fig. 6). This implies that until continental crust could accumulate to sufficient thickness, there would be little impetus to keep plate ages and the Wilson cycle within the several 100 Myr time frame; instead, with thin crust, plates would persist with a normal geometry for of order 1 Gyr before becoming unstable. That we currently see little evidence for plate ages older than about 200 Myrs suggests that it is possibly a result of accumulated continent mass making the plates unstable once they get much older than a few 100 Myrs.

4. Discussion

4.1. Observables and model predictions

Taken at face value our simple model predicts the order and timing of rollback versus detachment, specifically that the most significant rollback happens after detachment because of the loss of the plate driving force, which thus causes the plate to slow down and founder. However, there are various caveats to consider when making this interpretation. Most importantly, the model treats both rollback and detachment as being initiated by the same trigger, i.e., the accumulation of continental crust plugging up the subduction zone by imposing drag on the plate. However, rollback can have several causes including slabs impinging on a more viscous lower mantle, and thus, for example, stalling and flattening in the transition zone. This initial impingement on the lower mantle could both induce the plate to slow down and roll back, and also possibly inhibit an incipient necking instability by increasing viscous support of the slab's weight. However, our model assumes the slab has already penetrated into the lower mantle, and thus is most relevant for slabs extending below the transition zone. Therefore, any interpretation about the connection between detachment and rollback needs to infer whether rollback was already occurring by other mechanisms. While our model does propose that accumulation of continent itself causes some mild rollback by slowing the plate a bit, this rollback could be obscured by any possible prior rollback caused by, for example, the slab stalling in the transition zone. The model primarily predicts that the continental accumulation eventually triggers detachment of deeper slabs, which then causes a burst of rollback activity that could be superposed on rollback that may already be occurring.

The most appropriate comparison to numerical results is perhaps to that of models of delamination and necking following continental collision (Ueda et al., 2012; Magni et al., 2013). For example, in one of the cases explored by Ueda et al. (2012, see Fig. 4), continental collision is followed first by a gradual delamination event (similar to our model's initial slow rollback), and then by abrupt slab detachment (as in our model), which subsequently triggers a backward jump in the subduction zone (that can be associated with our abrupt post-necking rollback).

The clearest observations for timing of necking and rollback are probably (1) rapid uplift and associated volcanism following detachment (since uplift is in principle relatively fast, at isostatic adjustment or rebound rates, once detachment occurs); and (2) the record of trench migration, from paleomagnetic reconstruction, or geologic relics of paleo-trenches, for slab rollback. However, again, the occurrence of rollback preceding detachment could enhance detachment-induced uplift relative to the case without any preceding rollback (Buiter et al., 2002).

4.2. Observations

The Mediterranean is one of the most well studied regions for instances of both slab rollback and detachment that are coincident with continental accumulation and mountain building (see, e.g., Wortel and Spakman, 2000; Zhu et al., 2012; van Hinsbergen et al., 2014; Faccenna et al., 2014). However, it is also one of the more geologically complex regions and thus probably beyond the scope of our simple model predictions. Nevertheless, it is worth reviewing the observations and to what extent our model is applicable to them. The Apennine/Calabrian

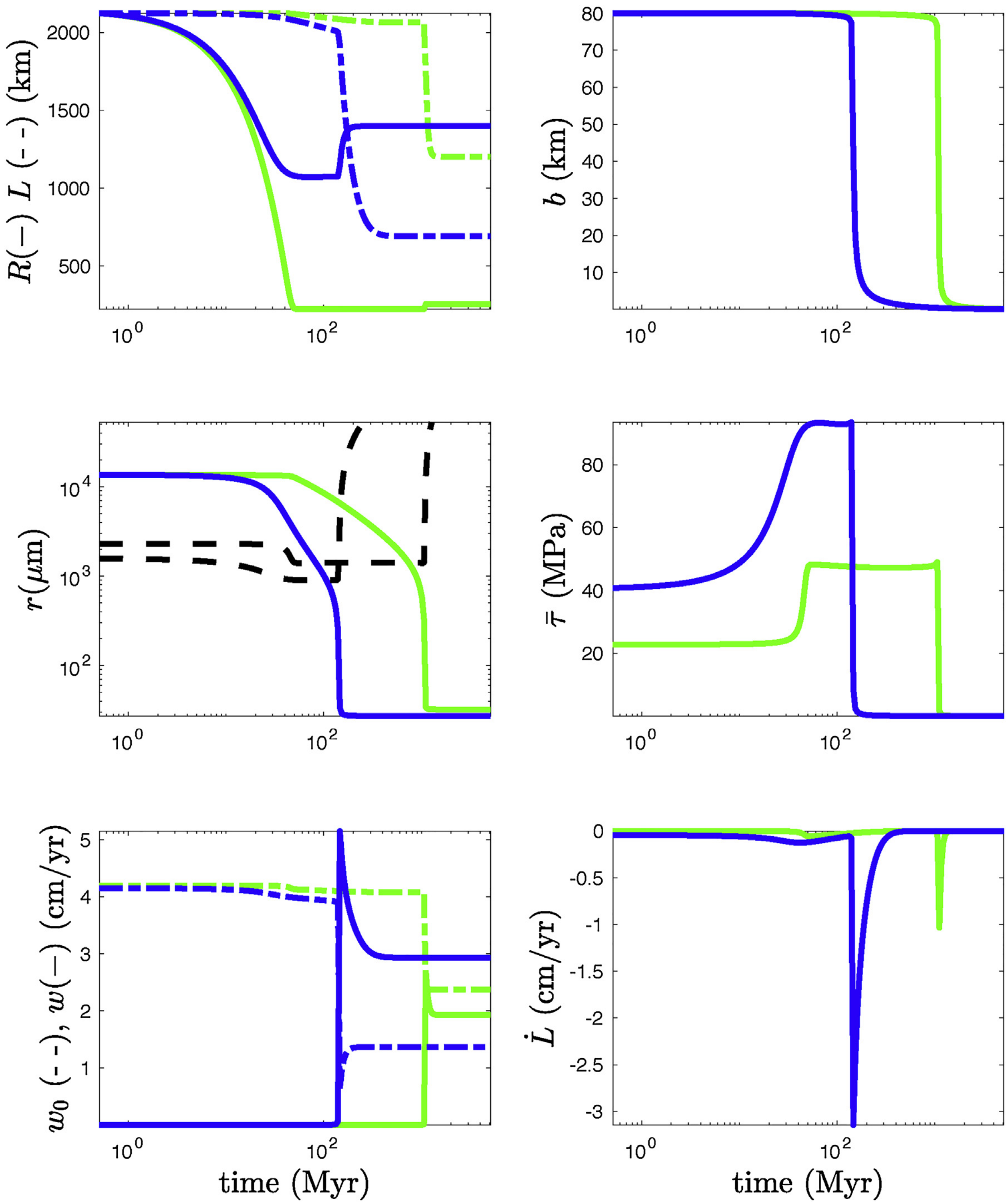

Fig. 6. Same as Fig. 5, but where now the colored curves show different average continental thickness h_c = 5 km (green) and 40 km (blue). (For interpretation of the references to color in this figure legend, the reader is referred to the web version of the article.)

system shows a well-recorded history of rollback and detachments, however the rollback proceeded for tens of millions of years before the detachment below the current position of the Apennine Range in the Italian peninsula. Likewise the Alpine/Carpathian system shows a consistent history of rollback (e.g., Schlunegger and Kissling, 2015), possibly followed by recent slab detachment, evident in rapid uplift in the Western Alps (Fox et al., 2015) and seismic anisotropy in the Eastern Alps (Qorbani et al., 2015). While our model predicts modest initial rollback, followed by detachment and then more rapid rollback, these observations indicate that the Mediterranean system experienced significant rollback first, before detachment. Indeed, Wortel and Spakman (2000) even argue that detachment would retard rollback, which is opposite to our model predictions. The Mediterranean is, however, complex with multiple subduction and collision systems occurring in a narrow region. Moreover, the first stage of rollback may be caused by other factors (e.g., lower mantle impedance of the slab; see Zhu et al., 2012) and thus would have been ongoing before the stress that would have triggered detachment. Thus, our simple 2D toy model has limited applicability to this system, and perhaps at best predicts that extant rollback might be accelerated after detachment, although this could be obviated by the complicated crustal structure and that rollback is propagating into continental crust rather than away from it. In short, while the Mediterranean is a classic system, it might just be too complex to compare to our simple model.

The western region of the India-Asia collision zone is a modern example of a convergent margin with temporally correlated continental thickening, slab detachment and trench rollback. Recent work including high-resolution tomography, analysis of deep seismicity and geological reconstructions, indicates shortening and thickening of the Gondwana crust, followed by stretching and detachment of the underlying slab beneath the Hindu Kush (Kufner et al., 2016). Specifically, Kufner et al. (2016) propose that, in the last ~10 Myr, the Indian cratonic lithosphere impinged on and under-thrusted Pamir, squeezing and thickening the rheologically weak overlying Gondwana crust. This collision triggered delamination and rollback of the Asian cratonic lithosphere, thus forming the Pamir slab, and initiated tearing and detachment of the Hindu Kush slab beneath the western margin of India. Thus, continental congestion of the subduction zone triggered both rollback and detachment. However, the geological system is significantly more complex than our toy model set-up, given the multiple slabs and the close proximity of two cratonic lithospheres (Indian and Asian) undergoing collision.

The most applicable cases for our model are possibly in the Western United States, where the continental margin and subduction systems are somewhat less complicated by curvature and convoluted crustal structure. First, in the American Pacific Northwest, the Cascadia subduction system experienced an increase in rollback rate around ~17 Ma, roughly coincident with the Columbia River Basin flood basalts (CRB) (Atwater and Stock, 1998; Long et al., 2012). Whether the CRB was initiated by a plume head or subduction-induced back-arc upwelling is still debated (Camp and Hanan, 2008; Obrebski et al., 2010; Faccenna et al., 2010; Liu and Stegman, 2012; Long, 2016). Slab detachment could have induced rapid mantle upwelling and concomitant volcanism, especially since USArray tomography shows that the old Farallon slab is fragmented (Obrebski et al., 2011; James et al., 2011; Long, 2016; Cheng et al., 2017), which could be evidence for detachment.

In the southwest of North America, there is evidence of Farallon slab detachment in Baja California (Brothers et al., 2012), possibly preceding trench migration and transtensional opening that helped create the peninsula (Atwater and Stock, 1998). Moreover, in Central Mexico there is evidence of slab detachment from volcanism, as well as migration of the volcanic front, which is indicative of rollback (Ferrari, 2004). In this case, rollback immediately followed detachment, as predicted in our model.

5. Summary and conclusion

We have presented a simple toy model for how continental accumulation and congestion of a subduction zone triggers coupled rollback and slab detachment. The model predicts that there is modest rollback at first due to increased continental drag on the plate. Once the stress from continental drag reaches its maximum, it triggers abrupt necking and slab detachment, augmented by grain-damage. The loss of the detached slab then causes the plate velocity to decrease, which then causes a rapid rollback event. After rollback the contracted continent then re-expands (because of the slower plate velocity), which is vaguely akin to continent dispersal, or at least the beginning stages of it.

Plausible model grain-damage parameters give feasible times for the speed, age and length of a plate before going unstable to necking and rollback. Moreover, typical 40 km thick continental crust likewise yields plates that last hundreds of Myrs before going unstable; however, thinner crust causes weak triggering of detachment and rollback and thus plates last billions of years before going unstable, which is obviously not evident in the current geological record, but is perhaps applicable to a much younger Earth.

Given the simplicity of the model, and that it does not account for all causes of rollback (such as slabs stalling in the mantle transition zone), it can only make predictions limited to simpler geological settings, involving less curved margins and unconvoluted crustal structure. Perhaps the best case studies are in Western North American, which has a few examples displaying (or possibly displaying) a significant phase of rollback following slab detachment.

Acknowledgments

The authors are very grateful to Taras Gerya and Scott King for their thoughtful reviews. This work was supported by National Science Foundation Grants EAR-1135382 (for DB and EM) and EAR-1150722 (for ML).

References

Atwater, T., Stock, J., 1998. Pacific-North America plate tectonics of the Neogene southwestern United States: an update. Int. Geol. Rev. 40 (5), 375–402. http://dx.doi.org/10.1080/00206819809465216.

Austin, N., Evans, B., 2007. Paleowattmeters: a scaling relation for dynamically recrystallized grain size. Geology 35, 343–346.

Becker, T., Conrad, C., Buffett, B., Müller, R., 2009. Past and present seafloor age distributions and the temporal evolution of plate tectonic heat transport. Earth Planet. Sci. Lett. 278, 233–242.

Bercovici, D., Long, M.D., 2014. Slab rollback instability and supercontinent dispersal. Geophys. Res. Lett. 41, 6659–6666. http://dx.doi.org/10.1002/2014GL061251.

Bercovici, D., Ricard, Y., 2012. Mechanisms for the generation of plate tectonics by two-phase grain-damage and pinning. Phys. Earth Planet. Int. 202-203, 27–55.

Bercovici, D., Ricard, Y., 2013. Generation of plate tectonics with two-phase grain-damage and pinning: source–sink model and toroidal flow. Earth Planet. Sci. Lett. 365, 275–288.

Bercovici, D., Ricard, Y., 2016. Grain-damage hysteresis and plate-tectonic states. Phys. Earth Planet. Int. 253, 31–47.

Bercovici, D., Schubert, G., Ricard, Y., 2015a. Abrupt tectonics and rapid slab detachment with grain damage. Proc. Natl. Acad. Sci. U. S. A. 112 (5), 1287–1291.

Bercovici, D., Schubert, G., Tackley, P.J., 1993. On the penetration of the 660 km phase change by mantle downflows. Geophys. Res. Lett. 20 (23), 2599–2602. http://dx.doi.org/10.1029/93GL02691.

Bercovici, D., Skemer, P., 2017. Grain damage, phase mixing and plate-boundary formation. J. Geodyn. 108, 40–55.

Bercovici, D., Tackley, P.J., Ricard, Y., 2015b. The generation of plate tectonics from mantle dynamics. In: David Bercovici (Gerald Schubert editor-in-chief) (Ed.), Treatise on Geophysics, vol. 7. Mantle Dynamics, 2nd edition. Elsevier, pp. 271–318 (Chapter 7).

Bevis, M., 1986. The curvature of Wadati–Benioff zones and the torsional rigidity of subducting plates. Nature 323, 52–53. http://dx.doi.org/10.1038/323052a0.

Bevis, M., 1988. Seismic slip and down-dip strain rates in Wadati–Benioff zones. Science 240 (4857), 1317–1319. http://science.sciencemag.org/content/240/4857/1317.

Billen, M.I., 2008. Modeling the dynamics of subducting slabs. Annu. Rev. Earth Planet. Sci. 36 (1), 325–356. http://dx.doi.org/10.1146/annurev.earth.36.031207.124129.

Billen, M.I., Hirth, G., 2007. Rheologic controls on slab dynamics. Geochem. Geophys. Geosyst. 8 (8). http://dx.doi.org/10.1029/2007GC001597.

Brothers, D., Harding, A., González-Fernández, A., Holbrook, W.S., Kent, G., Driscoll, N., Fletcher, J., Lizarralde, D., Umhoefer, P., Axen, G., 2012. Farallon slab detachment and deformation of the Magdalena Shelf, southern Baja California. Geophys. Res. Lett. 39 (9), l09307. http://dx.doi.org/10.1029/2011GL050828.

Buffett, B.A., 2006. Plate force due to bending at subduction zones. J. Geophys. Res. Solid Earth 111 (B9), b09405. http://dx.doi.org/10.1029/2006JB004295.

Buffett, B.A., Becker, T.W., 2012. Bending stress and dissipation in subducted lithosphere. J. Geophys. Res. Solid Earth 117. http://dx.doi.org/10.1029/2012JB009205.

Buffett, B.A., Rowley, D.B., 2006. Plate bending at subduction zones: consequences for the direction of plate motions. Earth Planet. Sci. Lett. 245 (1), 359–364. http://www.sciencedirect.com/science/article/pii/S0012821X06002160.

Buiter, S.J., Govers, R., Wortel, M., 2002. Two-dimensional simulations of surface deformation caused by slab detachment. Tectonophysics 354 (3), 195–210. http://www.sciencedirect.com/science/article/pii/S0040195102003360.

Burkett, E.R., Billen, M.I., 2010. Three-dimensionality of slab detachment due to ridge-trench collision: laterally simultaneous boudinage versus tear propagation. Geochem. Geophys. Geosyst. 11 (11). http://dx.doi.org/10.1029/2010GC003286.

Camp, V.E., Hanan, B.B., 2008. A plume-triggered delamination origin for the Columbia River Basalt Group. Geosphere 4 (3), 480. http://dx.doi.org/10.1130/GES00175.1.

Chandrasekhar, S., 1961. Hydrodynamic and Hydromagnetic Stability. Oxford University Press, New York.

Cheng, C., Bodin, T., Tauzin, B., Allen, R.M., 2017. Cascadia subduction slab heterogeneity revealed by three-dimensional receiver function Kirchhoff migration. Geophys. Res. Lett. 44 (2), 694–701. http://dx.doi.org/10.1002/2016GL072142. 2016GL072142.

Clark, S.R., Stegman, D., Müller, R.D., 2008. Episodicity in back-arc tectonic regimes. Phys. Earth Planet. Interiors 171 (1–4), 265–279. http://www.sciencedirect.com/science/article/pii/S0031920108000836.

Clift, P., Lin, J., Barckhausen, U., 2002. Evidence of low flexural rigidity and low viscosity lower continental crust during continental break-up in the South China Sea. Mar. Pet. Geol. 19 (8), 951–970. http://www.sciencedirect.com/science/article/pii/S0264817202001083.

Coltice, N., Rolf, T., Tackley, P.J., Labrosse, S., 2012. Dynamic causes of the relation

between area and age of the ocean floor. Science 336 (6079), 335–338. http://www.sciencemag.org/content/336/6079/335.abstract.
Conrad, C., Hager, B., 2001. Mantle convection with strong subduction zones. Geophys. J. Int. 144, 271–288.
Crameri, F., Tackley, P.J., 2014. Spontaneous development of arcuate single-sided subduction in global 3-D mantle convection models with a free surface. J. Geophys. Res. Solid Earth. http://dx.doi.org/10.1002/2014JB010939.
Cross, A., Skemer, P., 2017. Ultramylonite generation via phase mixing in high strain experiments. J. Geophys. Res. Solid Earth 122, 1744–1759.
Didden, N., Maxworthy, T., 1982. The viscous spreading of plane and axisymmetric gravity currents. J. Fluid Mech. 121, 27–42.
Duretz, T., Gerya, T.V., May, D.A., 2011. Numerical modelling of spontaneous slab breakoff and subsequent topographic response. Tectonophysics 502 (1), 244–256. http://www.sciencedirect.com/science/article/pii/S0040195110002416.
Duretz, T., Schmalholz, S.M., Gerya, T.V., 2012. Dynamics of slab detachment. Geochem. Geophys. Geosyst. 13 (3). http://dx.doi.org/10.1029/2011GC004024.
Evans, B., Renner, J., Hirth, G., 2001. A few remarks on the kinetics of static grain growth in rocks. Int. J. Earth Sci. (Geol. Rundsch.) 90, 88–103.
Faccenna, C., Becker, T.W., Auer, L., Billi, A., Boschi, L., Brun, J.P., Capitanio, F.A., Funiciello, F., Horvàth, F., Jolivet, L., Piromallo, C., Royden, L., Rossetti, F., Serpelloni, E., 2014. Mantle dynamics in the Mediterranean. Rev. Geophys. 52 (3), 283–332. http://dx.doi.org/10.1002/2013RG000444. 2013RG000444.
Faccenna, C., Becker, T.W., Lallemand, S., Lagabrielle, Y., Funiciello, F., Piromallo, C., 2010. Subduction-triggered magmatic pulses: a new class of plumes? Earth Planet. Sci. Lett. 299 (1), 54–68. http://www.sciencedirect.com/science/article/pii/S0012821X10005224.
Ferrari, L., 2004. Slab detachment control on mafic volcanic pulse and mantle heterogeneity in central Mexico. Geology 32 (1), 77. http://dx.doi.org/10.1130/G19887.1.
Foley, B.J., Bercovici, D., Landuyt, W., 2012. The conditions for plate tectonics on super-earths: inferences from convection models with damage. Earth Planet. Sci. Lett. 331-332, 281–290.
Forsyth, D., Uyeda, S., 1975. On the relative importance of the driving forces of plate motion. Geophys. J. R. Astron. Soc. 43, 163–200.
Fox, M., Herman, F., Kissling, E., Willett, S.D., 2015. Rapid exhumation in the Western Alps driven by slab detachment and glacial erosion. Geology 43 (5), 379. http://dx.doi.org/10.1130/G36411.1.
Funiciello, F., Moroni, M., Piromallo, C., Faccenna, C., Cenedese, A., Bui, H.A., 2006. Mapping mantle flow during retreating subduction: laboratory models analyzed by feature tracking. J. Geophys. Res. Solid Earth 111 (B3). http://dx.doi.org/10.1029/2005JB003792.
Gerya, T.V., Meilick, F.I., 2011. Geodynamic regimes of subduction under an active margin: effects of rheological weakening by fluids and melts. J. Metamorph. Geol. 29 (1), 7–31. http://dx.doi.org/10.1111/j.1525-1314.2010.00904.x.
Gerya, T.V., Yuen, D.A., Maresch, W.V., 2004. Thermomechanical modelling of slab detachment. Earth Planet. Sci. Lett. 226 (1), 101–116. http://www.sciencedirect.com/science/article/pii/S0012821X0400456X.
Gurnis, M., 1990. Bounds on global dynamic topography from phanerozoic flooding of continental platforms. Nature 344, 754–756.
Gurnis, M., 1993. Phanerozoic marine inundation of continents driven by dynamic topography above subducting slabs. Nature 364, 589–593.
Gurnis, M., Hager, B., 1988. Controls of the structure of subducted slabs. Nature 335, 317–321.
Hiraga, T., Tachibana, C., Ohashi, N., Sano, S., 2010. Grain growth systematics for forsterite ± enstatite aggregates: effect of lithology on grain size in the upper mantle. Earth Planet. Sci. Lett. 291, 10–20.
Hirth, G., Kohlstedt, D., 2003. Rheology of the upper mantle and the mantle wedge: a view from the experimentalists. In: In: Eiler, J. (Ed.), Subduction Factor Mongraph, vol. 138. Am. Geophys. Union, Washington, DC, pp. 83–105.
Howard, L.N., 1966. Convection at high Rayleigh number. In: Gortler, H. (Ed.), Proceedings of the Eleventh International Congress of Applied Mechanics. Springer-Verlag, New York, pp. 1109–1115.
Huppert, H., 1982. The propagation of two-dimensional and axisymmetric viscous gravity currents over a rigid horizontal surface. J. Fluid Mech. 121, 43–58.
Jadamec, M.A., Billen, M.I., 2010. Reconciling surface plate motions with rapid three-dimensional mantle flow around a slab edge. Nature 465, 338EP. http://dx.doi.org/10.1038/nature09053.
Jadamec, M.A., Billen, M.I., 2012. The role of rheology and slab shape on rapid mantle flow: three-dimensional numerical models of the Alaska slab edge. J. Geophys. Res. Solid Earth (1978–2012) 117 (B2). http://dx.doi.org/10.1029/2011JB008563.
James, D.E., Fouch, M.J., Carlson, R.W., Roth, J.B., 2011. Slab fragmentation, edge flow and the origin of the Yellowstone hotspot track. Earth Planet. Sci. Lett. 311 (1), 124–135. http://www.sciencedirect.com/science/article/pii/S0012821X11005188.
Karato, S., 1989. Grain growth kinetics in olivine aggregates. Tectonophysics 168, 255–273.
Karato, S., Toriumi, M., Fujii, T., 1980. Dynamic recrystallization of olivine single crystals during high temperature creep. Geophys. Res. Lett. 7, 649–652.
Kincaid, C., Griffiths, R.W., 2003. Laboratory models of the thermal evolution of the mantle during rollback subduction. Nature 425 (6953), 58–62. http://dx.doi.org/10.1038/nature01923.
Kirby, S.H., Kronenberg, A.K., 1987. Rheology of the lithosphere: selected topics. Rev. Geophys. 25 (6), 1219–1244. http://dx.doi.org/10.1029/RG025i006p01219.
Kohlstedt, D., Evans, B., Mackwell, S., 1995. Strength of the lithosphere: constraints imposed by laboratory experiments. J. Geophys. Res. 100, 17587–17602.
Kufner, S.-K., Schurr, B., Sippl, C., Yuan, X., Ratschbacher, L., s/of Mohammad Akbar, A., Ischuk, A., Murodkulov, S., Schneider, F., Mechie, J., Tilmann, F., 2016. Deep India meets deep Asia: lithospheric indentation, delamination and break-off under Pamir and Hindu Kush (Central Asia). Earth Planet. Sci. Lett. 435, 171–184. http://www.sciencedirect.com/science/article/pii/S0012821X15007505.
Labrosse, S., Jaupart, C., 2007. Thermal evolution of the earth: secular changes and fluctuations of plate characteristics. Earth Planet. Sci. Lett. 260 (3), 465–481. http://www.sciencedirect.com/science/article/pii/S0012821X07003615.
Lallemand, S., Heuret, A., Faccenna, C., Funiciello, F., 2008. Subduction dynamics as revealed by trench migration. Tectonics 27 (3). http://dx.doi.org/10.1029/2007TC002212.
Lee, C., King, S.D., 2011. Dynamic buckling of subducting slabs reconciles geological and geophysical observations. Earth Planet. Sci. Lett. 312 (3), 360–370. http://www.sciencedirect.com/science/article/pii/S0012821X11006315.
Linckens, J., Bruijn, R.H., Skemer, P., 2014. Dynamic recrystallization and phase mixing in experimentally deformed peridotite. Earth Planet. Sci. Lett. 388, 134–142.
Liu, L., Stegman, D.R., 2012. Origin of Columbia River flood basalt controlled by propagating rupture of the Farallon slab. Nature 482 (February (7385)), 386–389. http://dx.doi.org/10.1038/nature10749.
Long, M.D., 2016. The Cascadia paradox: mantle flow and slab fragmentation in the Cascadia subduction system. J. Geodyn. 102, 151–170. http://www.sciencedirect.com/science/article/pii/S0264370716301284.
Long, M.D., Becker, T., 2010. Mantle dynamics and seismic anisotropy. Earth Planet. Sci. Lett. 297 (3–4), 341–354.
Long, M.D., Silver, P.G., 2009. Mantle flow in subduction systems: the subslab flow field and implications for mantle dynamics. J. Geophys. Res. Solid Earth 114 (B10). http://dx.doi.org/10.1029/2008JB006200.
Long, M.D., Till, C.B., Druken, K.A., Carlson, R.W., Wagner, L.S., Fouch, M.J., James, D.E., Grove, T.L., Schmerr, N., Kincaid, C., 2012. Mantle dynamics beneath the Pacific Northwest and the generation of voluminous back-arc volcanism. Geochem. Geophys. Geosyst. 13 (8). http://dx.doi.org/10.1029/2012GC004189.
Magni, V., Faccenna, C., Hunen, J., Funiciello, F., 2013. Delamination vs. break-off: the fate of continental collision. Geophys. Res. Lett. 40 (2), 285–289. http://dx.doi.org/10.1002/grl.50090.
Meissner, R., 1986. The Continental Crust: A Geophysical Approach, vol. 34 of International Geophysics Series. Academic Press, London.
Moresi, L., Betts, P.G., Miller, M.S., Cayley, R.A., 2014. Dynamics of continental accretion. Nature 508 (7495), 245–248. http://dx.doi.org/10.1038/nature13033.
Mulyukova, E., Bercovici, D., 2017. Formation of lithospheric shear zones: effect of temperature on two-phase grain damage. Phys. Earth Planet. Interiors 270, 195–212. http://www.sciencedirect.com/science/article/pii/S0031920117300821.
Mulyukova, E., Bercovici, D., 2018. Collapse of passive margins by lithospheric damage and plunging grain size. Earth Planet. Sci. Lett. 484, 341–352. https://www.sciencedirect.com/science/article/pii/S0012821X17307331.
Obrebski, M., Allen, R.M., Pollitz, F., Hung, S.-H., 2011. Lithosphere-asthenosphere interaction beneath the western United States from the joint inversion of body-wave traveltimes and surface-wave phase velocities. Geophys. J. Int. 185 (2), 1003–1021. http://dx.doi.org/10.1111/j.1365-246X.2011.04990.x.
Obrebski, M., Allen, R.M., Xue, M., Hung, S.-H., 2010. Slab-plume interaction beneath the Pacific Northwest. Geophys. Res. Lett. 37 (14), l14305. http://dx.doi.org/10.1029/2010GL043489.
Piromallo, C., Becker, T.W., Funiciello, F., Faccenna, C., 2006. Three-dimensional instantaneous mantle flow induced by subduction. Geophys. Res. Lett. 33 (8). http://dx.doi.org/10.1029/2005GL025390.
Qorbani, E., Bianchi, I., Bokelmann, G., 2015. Slab detachment under the Eastern Alps seen by seismic anisotropy. Earth Planet. Sci. Lett. 409, 96–108. http://www.sciencedirect.com/science/article/pii/S0012821X14006761.
Rey, P., Vanderhaeghe, O., Teyssier, C., 2001. Gravitational collapse of the continental crust: definition, regimes and modes. Tectonophysics 342 (3), 435–449. http://www.sciencedirect.com/science/article/pii/S0040195101001743.
Ribe, N., Stutzmann, E., Ren, Y., van der Hilst, R., 2007. Buckling instabilities of subducted lithosphere beneath the transition zone. Earth Planet. Sci. Lett. 254 (1), 173–179. http://www.sciencedirect.com/science/article/pii/S0012821X06008466.
Ribe, N.M., Sep 2003. Periodic folding of viscous sheets. Phys. Rev. E 68, 036305. http://dx.doi.org/10.1103/PhysRevE.68.036305.
Richards, M., Yang, W.-S., Baumgardner, J., Bunge, H.-P., 2001. Role of a low-viscosity zone in stabilizing plate tectonics: implications for comparative terrestrial planetology. Geochem. Geophys. Geosyst. (G^3) 2 2000GC000115.
Rogers, R., Karason, H., van der Hilst, R., NOV 2002. Epeirogenic uplift above a detached slab in northern Central America. Geology 30 (11), 1031–1034.
Rozel, A., Ricard, Y., Bercovici, D., 2011. A thermodynamically self-consistent damage equation for grain size evolution during dynamic recrystallization. Geophys. J. Int. 184 (2), 719–728.
Schellart, W., Stegman, D., Freeman, J., 2008. Global trench migration velocities and slab migration induced upper mantle volume fluxes: constraints to find an earth reference frame based on minimizing viscous dissipation. Earth Sci. Rev. 88 (1–2), 118–144. http://www.sciencedirect.com/science/article/pii/S0012825208000184.
Schellart, W.P., Freeman, J., Stegman, D.R., Moresi, L., May, D., 2007. Evolution and diversity of subduction zones controlled by slab width. Nature 446 (7133), 308–311. http://dx.doi.org/10.1038/nature05615.
Schlunegger, F., Kissling, E., 2015. Slab rollback orogeny in the Alps and evolution of the Swiss Molasse basin. Nat. Commun. 10, 8605EP. http://dx.doi.org/10.1038/ncomms9605.
Schmalholz, S.M., 2011. A simple analytical solution for slab detachment. Earth Planet. Sci. Lett. 304, 45–54.
Schott, B., Schmeling, H., 1998. Delamination and detachment of a lithospheric root. Tectonophysics 296 (3–4), 225–247.
Schubert, G., 1980. Self-driven motions of plates and descending slabs. In: Davies, P., Runcorn, S. (Eds.), Mechanisms of Continental Drift and Plate Tectonics. Academic

Press, pp. 151–158.
Schubert, G., Turcotte, D., Olson, P., 2001. Mantle Convection in the Earth and Planets. Cambridge Univ. Press.
Schubert, G., Turcotte, D., Yuen, D., 1975. Role of phase transitions in a dynamic mantle. Geophys. J. R. Astron. Soc 42, 705–735.
Solomatov, V., 1995. Scaling of temperature dependent and stress dependent viscosity convection. Phys. Fluids 7, 266–274.
Stegman, D., Farrington, R., Capitanio, F., Schellart, W., 2010. A regime diagram for subduction styles from 3-D numerical models of free subduction. Tectonophysics 483 (1–2), 29–45. http://www.sciencedirect.com/science/article/pii/S0040195109004776.
Stegman, D.R., Freeman, J., Schellart, W.P., Moresi, L., May, D., 2006. Influence of trench width on subduction hinge retreat rates in 3-D models of slab rollback. Geochem. Geophys. Geosyst. 7 (3). http://dx.doi.org/10.1029/2005GC001056.
Tackley, P., Stevenson, D., Glatzmaier, G.A., Schubert, G., 1993. Effects of an endothermic phase transition at 670 km depth in a spherical model of convection in the earth's mantle. Nature 361, 699–704.
Tao, W.C., O'Connell, R.J., 1993. Deformation of a weak subducted slab and variation of seismicity with depth. Nature 361, 626–628. http://dx.doi.org/10.1038/361626a0.
Turcotte, D., Oxburgh, E., 1967. Finite amplitude convection cells and continental drift. J. Fluid Mech. 28, 29–42.
Turcotte, D., Schubert, G., 2014. Geodynamics. Cambridge University Press, Cambridge, UK.
Ueda, K., Gerya, T.V., Burg, J., 2012. Delamination in collisional orogens: thermomechanical modeling. J. Geophys. Res. Solid Earth (1978–2012) 117 (B8). http://dx.doi.org/10.1029/2012JB009144.
van Hinsbergen, D.J.J., Vissers, R.L.M., Spakman, W., 2014. Origin and consequences of western Mediterranean subduction, rollback, and slab segmentation. Tectonics 33 (4), 393–419. http://dx.doi.org/10.1002/2013TC003349. 2013TC003349.
van Hunen, J., Allen, M.B., 2011. Continental collision and slab break-off: a comparison of 3-D numerical models with observations. Earth Planet. Sci. Lett. 302 (1), 27–37. http://www.sciencedirect.com/science/article/pii/S0012821X10007429.
Vergnolle, M., Pollitz, F., Calais, E., 2003. Constraints on the viscosity of the continental crust and mantle from GPS measurements and postseismic deformation models in western Mongolia. J. Geophys. Res. Solid Earth 108 (B10), 2502. http://dx.doi.org/10.1029/2002JB002374.
Vigny, C., Ricard, Y., Froidevaux, C., 1991. The driving mechanism of plate tectonics. Tectonophysics 187, 345–360.
Wada, I., King, S.D., 2015. Dyamics of subducting slabs: numerical modeling and constraints from seismology, geoid, topography, geochemistry and petrology. In: David Bercovici (Gerald Schubert editor-in-chief) (Ed.), Treatise on Geophysics, vol. 7. Mantle Dynamics, 2nd edition. Elsevier, pp. 339–392 (Chapter 9).
Wortel, M., Spakman, W., DEC 8 2000. Subduction and slab detachment in the Mediterranean-Carpathian region. Science 290 (5498), 1910–1917.
Zhu, H., Bozdag, E., Peter, D., Tromp, J., 2012. Structure of the European upper mantle revealed by adjoint tomography. Nat. Geosci. 5 (7), 493–498.